

Strategies for Strengthening Zn Metal Anodes in Aqueous Zinc-Ion Batteries—Current States and Perspectives

Shuo Liu, Xiaoyue Li, Mengyao Qin, Shuyang Bian, Fei Ye, Yuping Wu, Wenshu Chen,* Pan Feng,* and Linfeng Hu*



Cite This: <https://doi.org/10.1021/acsaem.5c00640>



Read Online

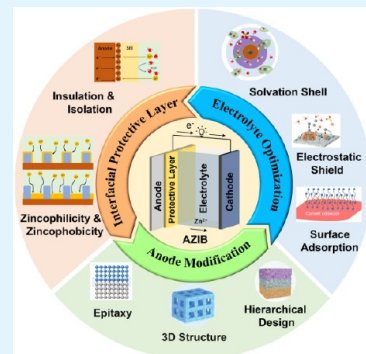
ACCESS |

Metrics & More

Article Recommendations

ABSTRACT: Aqueous zinc-ion batteries (AZIBs) stand out as a compelling alternative to their lithium-ion counterparts, boasting advantages such as cost-effectiveness, superior safety, and diminished environmental ramifications. Notwithstanding notable advancements in cathode materials for AZIBs, pivotal obstacles associated with the Zn metal anode remain largely underinvestigated, thus hindering their application in grid-scale storage, portable electronics, and so on. This review offers a comprehensive overview of the intrinsic challenges confronting Zn anodes in aqueous electrolytes, while also aggregating recent progress in mitigating these setbacks. Solutions are delineated across three paradigms: (1) strengthening Zn anodes through structural design, (2) enhancing Zn anodes by establishing protective layers, and (3) electrolyte optimization via additive incorporation and compositional adjustments. Each strategy undergoes rigorous scrutiny concerning its potential to curtail dendrite proliferation, impede parasitic HER, and bolster electrochemical resilience. Additionally, future research directions such as AI-driven optimization, high-entropy approaches, and bio-inspired strategies are discussed to advance high-performance AZIBs toward practical applications.

KEYWORDS: aqueous zinc-ion batteries, zn anode issues, structural design, protective layers, electrolyte optimization



1. INTRODUCTION

Lithium-ion batteries (LIBs) have dominated the market of electrochemical energy storage, owing to their high efficiency, energy density, and longevity. However, the use of nonaqueous electrolytes, which are both inflammable and detrimental to the environment, poses significant safety concerns.^{1,2} Furthermore, the high cost, scarcity of lithium resources, and inherent security risks make LIBs unsuitable for large-scale energy storage systems.³ In response, aqueous zinc-ion batteries (AZIBs) have been proposed as a next-generation green energy storage solution. Zinc's primary advantage is its electrochemical redox voltage (-0.76 V vs SHE),⁴ which aligns well with the stable potential window of water, allowing it to function directly as the anode in the aqueous electrolyte. This aqueous electrolyte not only enhances the safety features of AZIBs but also improves their ionic conductivity compared to LIBs. Moreover, due to their low cost, abundant reserves, high theoretical specific capacity (gravimetric capacities of 820 mAh g⁻¹ and volumetric capacities of 5855 mAh cm⁻³, respectively),⁵ environmental friendliness, and good reversibility in aqueous environments, ZIBs are gaining recognition as promising batteries for grid-scale storage. To date, extensive research on aqueous zinc-ion batteries has been documented, covering zinc metal anodes, cathodes, electrolytes, and their potential applications among others. However, the unresolved issues associated with zinc anodes continue to impose

inevitable adverse effects on the cycling stability and critical performance metrics of the full battery system, thereby significantly hindering the advancement of its commercialization.

2. FUNDAMENTALS AND KEY CHALLENGES OF ZN ANODE

Unlike lithium-ion, sodium-ion, and potassium-ion batteries, zinc metal can be directly utilized as the anode owing to its inherent electrochemical stability in aqueous environments. However, it remains confronted with formidable challenges that impede the commercialization (Figure 1a). Among these, Zn dendrite is a primary concern. Typically, AZIBs are fabricated using commercial Zn foil characterized by a nonuniform surface morphology with numerous protrusions observable under microscopic examination.^{6,7} During the AZIBs charging process, Zn²⁺ ions undergo heterogeneous nucleation and rapid crystallization at these surface protrusions. This tendency is amplified by the tip effect, where

Received: March 3, 2025

Revised: May 29, 2025

Accepted: May 30, 2025

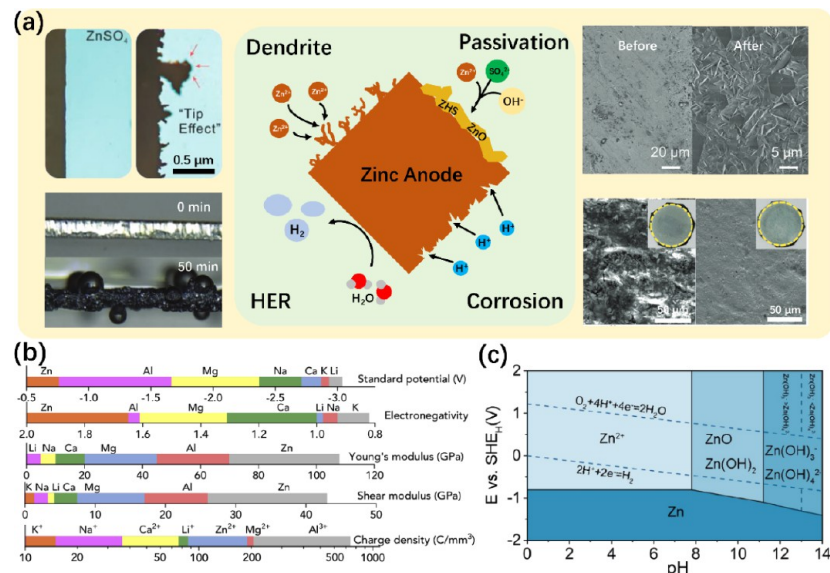


Figure 1. Fundamentals and key challenges of Zn anode. (a) Schematics of the dendrites, HER, passivation and corrosion issues on Zn anodes.^{10–13} Reproduced with permission from refs. ^{10–10}. Copyright 2023, John Wiley and Sons Inc. Copyright 2024, John Wiley and Sons Inc. Copyright 2024, John Wiley and Sons Inc. Copyright 2024, John Wiley and Sons Inc. Copyright 2021, Elsevier. (b) Physical and chemical properties of various metals and metal ions.⁸ Reproduced with permission from ref. ⁸. Copyright 2021, Elsevier. (c) The Pourbaix diagram of Zn in aqueous solution.¹⁴ Reproduced from ref. ¹⁰.

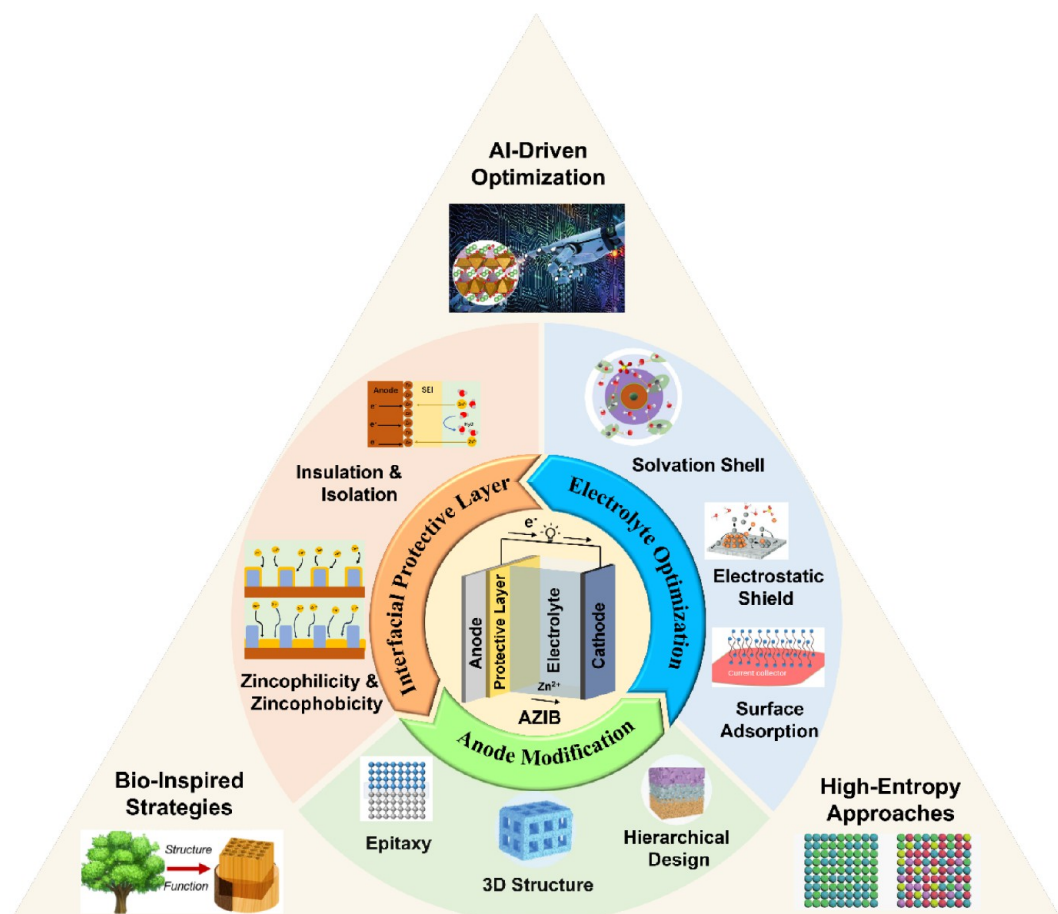


Figure 2. Developed strategies for strengthening Zn metal anodes in aqueous zinc-ion batteries.

electron accumulation at asperity tips creates a distorted, intensified electric field, further driving the preferential accumulation of Zn^{2+} ions toward these protruding regions

and leading to dendritic growth. However, a mismatch exists between the zinc-ion stripping and deposition rates in localized areas on the electrode surface during the discharge process.

This inconsistency inhibits the full dissolution of dendrites while simultaneously causing dendrite and void formation on the anode. Once the dendrites fracture and detach from the electrode, they induce irreversible specific capacity decay due to the loss of active material. Compared to other alkali metals, Zn has a notably higher Young's and shear modulus, leading to the creation of dendrites more likely to penetrate the separator, thereby posing significant safety risks (Figure 1b).⁸ The widely accepted diffusion model (eq 1) was developed to systematically measure the contributions of various influencing factors to dendritic growth dynamics.⁹

$$\tau = \frac{eC_0(\mu_a + \mu_{ion})^2}{2J\mu_a} \quad (1)$$

where τ is the time when the dendrites start to grow, D is the diffusion coefficient, e is the electronic charge, C_0 is the initial concentration of electrolytes, μ_a and μ_{ion} are the anionic and metal cation mobility, respectively, and J is the effective electrode current density. The electron transport process can influence the effective electrode current density (J) of the electrode, thereby impacting Sand's time (τ). Theoretical analysis indicates that increasing the diffusion rate of metal cations and reducing the local current density at the electrode interface may lengthen the incubation period for dendrite initiation. This elongation could potentially enhance the cycle life of rechargeable batteries.

In addition, the hydrogen evolution reaction (HER) is a frequent problem in aqueous ZIBs. From a thermodynamic perspective, the standard reduction potential of Zn^{2+}/Zn (-0.76 V vs SHE) is lower than the HER within a pH range of 1–14 (Figure 1c), suggesting that HER is thermodynamically favored over Zn deposition. More critically, the intense electric fields and increased contact area with the electrolyte, resulting from dendrite formation, intensify the occurrence of HER. The accumulation of hydrogen gas inside the battery can increase internal pressure, potentially leading to impaired interfacial contact between electrodes and contributing to battery failure.

In addition to the issues previously mentioned, Zn anodes encounter the challenges of corrosion and surface passivation. The primary concern arises from the marked pH sensitivity of these anodes. In strongly acidic environments, Zn rapidly dissolves into ionic species. Even in weakly acidic or neutral conditions, the sluggish reaction of Zn with H^+ or HER results in an increase in pH. Under neutral to weakly alkaline conditions, Zn undergoes a reactive transformation with the electrolyte, producing heterogeneous compounds such as ZnO , $Zn(OH)_2$, and $Zn_4(OH)_6SO_4$. Contrary to protecting the anode, these compounds, characterized by their loose structures, increase internal resistance and adversely affect both Coulombic efficiency and cycling performance.

This review offers a comprehensive examination of the fundamental challenges associated with Zn anodes in aqueous electrolytes, while also highlighting recent advancements made in overcoming these limitations. The strategies for enhancing the anode are detailed with particular focus on three critical components: the Zn anode structure, protective layer, and electrolyte design. Additionally, prospective insights into potential future research directions are provided.

3. ZN ANODE STRENGTHENING STRATEGIES

Over recent years, numerous strategies have been proposed to enhance the reversibility of Zn metal anodes in aqueous electrolytes. These strategies can be categorized into three distinct approaches based on their design philosophy and functional objectives (Figure 2): (i) Designing Zn anodes with specialized structures and meticulously engineered lattices. This approach focuses on modifying the microstructure and properties of the Zn anode to ensure more efficient and sustainable Zn storage. (ii) Introducing an additional layer on the Zn anode, primarily aimed at separating the Zn anode from the aqueous electrolyte while facilitating ion transport. This protective layer is predominantly designed to promote uniform ion deposition and suppress Zn dendrite formation rather than actively storing Zn. (iii) Refining the composition and concentration of the electrolyte. Given their role in battery interactions, electrolytes significantly influence the performance of the anode.

3.1. Zn Metal Structural Design. Recent literature reports suggest that the crystallographic orientation of electrode materials significantly impacts ion deposition behavior. This indicates that increased irregularity in crystallographic orientations at the electrode surface may correlate with a higher likelihood of disordered deposition patterns.^{6,7,15–18} The relative texture coefficients (RTC) can be defined by eq 2,¹⁵ which quantifies the degree of preferential crystallographic orientation in a polycrystalline material compared to a reference state.

$$RTC_{(hkl)} = \frac{I_{(hkl)}/\bar{I}_{(hkl)}}{\sum [I_{(hkl)}/\bar{I}_{(hkl)}]} \times 100 \quad (2)$$

In the (002), (100), and (101) crystal planes where RTC is high, the morphology of the newly deposited Zn metal is determined by the preferred crystal plane.¹⁸ Specifically, Zn deposits on substrates with (100)/(101) planes demonstrate a marked vertical growth component ($>60^\circ$), fostering dendrite growth. In contrast, epitaxial alignment with the (002) substrate plane encourages lateral horizontal growth ($<15^\circ$), leading to consistent layer-by-layer deposition. Moreover, the Zn (002) surface has been shown to offer superior corrosion resistance and dendrite suppression compared to the Zn (100) and (101) planes.¹⁶

Although the (002) crystal plane of Zn metal is widely regarded as more effective in suppressing anode side reactions and dendrite growth compared to other crystallographic facets, recent studies have demonstrated that certain other surfaces, such as the (100)^{19–21} and (101)^{13,22} planes, can also exhibit favorable electrochemical cycling performance. The critical current density (CCD) is defined as a critical parameter influencing dendrite formation and battery failure. When the current density exceeds the CCD, it signifies that the deposition rate of metallic ions surpasses the replenishment rate of ions at the interface. This results in amplified local current density at critical sites, driving dendrite nucleation and eventual battery failure.²³ Ren et al. demonstrated that while the (002) crystal plane of Zn exhibits a higher CCD compared to the (100) plane, the (100) plane achieves a larger critical areal capacity (CAC)—defined as the maximum areal capacity before short-circuiting occurs in Zn symmetric cells under a given current density.¹⁹ During deep discharge testing, the (001) crystal plane displayed superior reversibility relative to other crystal planes and all such single-crystal orientations

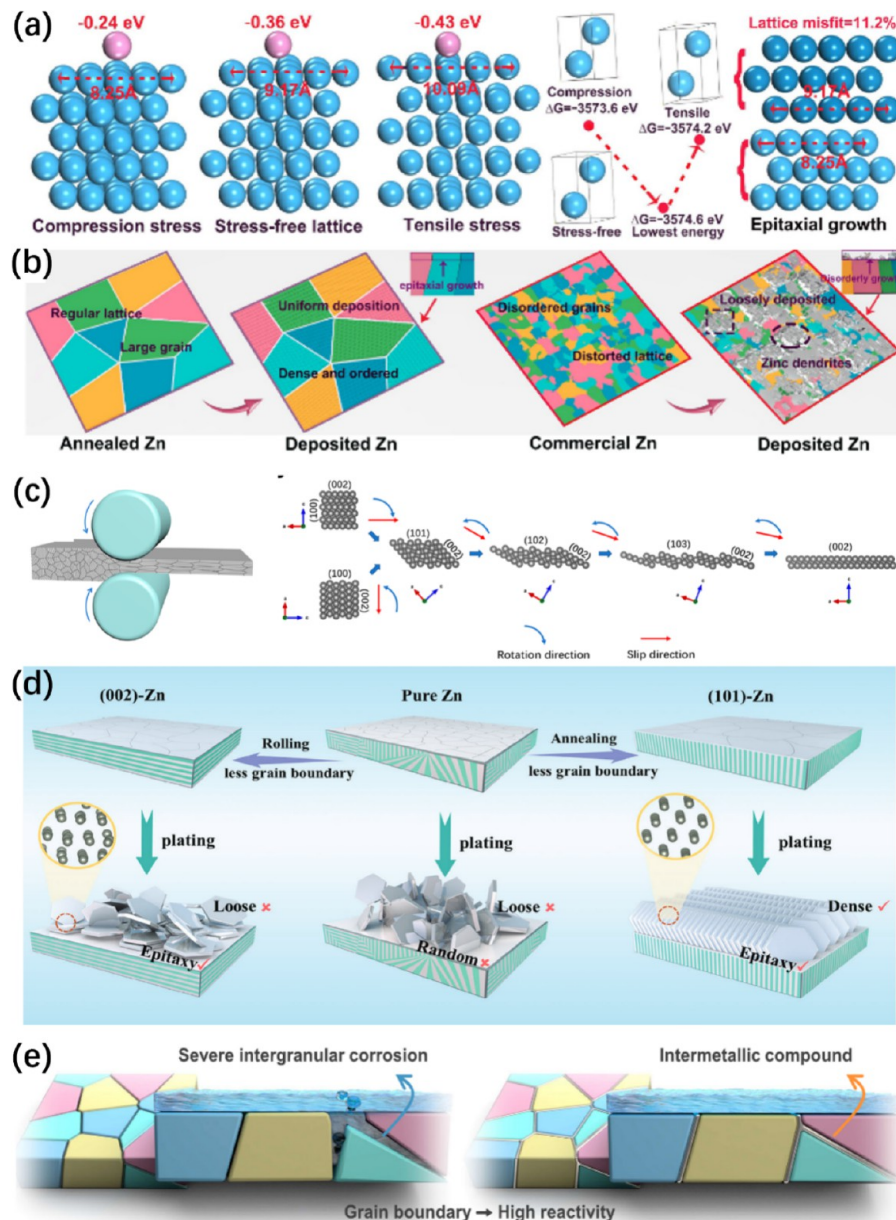


Figure 3. Challenges and process engineering solutions for commercial zinc foils. (a) Zn (002) facets and their binding energies to Zn atoms under different stress conditions.²⁴ (b) A schematic of Zn deposition on different substrates.²⁴ Reproduced with permission from ref. 24. Copyright 2023, John Wiley and Sons Inc. (c) A schematic of crystal plane evolution process during repeated cold-rolling.⁶ Reproduced from ref. 6. Copyright 2022, American Chemical Society (d) Schematic illustrations of Zn plating mechanism on pure Zn, (002)-Zn, and (101)-Zn anode.¹³ Reproduced with permission from ref. 13. Copyright 2023, John Wiley and Sons Inc. (e) Schematic illustration of the grain boundary engineering.²⁷ Reproduced from ref. 27.

outperformed polycrystalline Zn in terms of cycling stability. Based on the aforementioned findings, while individual Zn crystal planes exhibit disparities in electrochemical properties, the primary cause of anode degradation is typically attributed to the heterogeneous orientation of polycrystalline planes.

Additionally, factors such as grain size, grain boundaries, lattice defects, and residual stresses in commercial Zn foils—parameters that often fluctuate between different batches—exert a significant influence on the electrochemical deposition process. Recent research has shown that these foils typically display randomized crystallographic orientations, high density of lattice defects (e.g., dislocations and vacancies), and residual stresses. These inherent microstructural heterogeneities contribute to the underperformance of commercial Zn foils

in electrochemical tests, including accelerated corrosion and uneven Zn stripping/plating (Figure 3a,b).^{7,17,24} To mitigate these issues, conventional metallurgical processing techniques such as rolling, annealing, and melt recrystallization have been employed (Figure 3c and Table 1). These techniques effectively reduce residual stress and lattice defect density while promoting abnormal grain growth and inducing a highly preferred (002) plane.^{6,7,17,18,24} However, Liu et al. argued that the (002) crystal plane exhibits weaker bonding interactions with deposited atoms. Consequently, Zn deposited on textured (002)-oriented substrates tends to deviate from its original lattice growth pattern, leading to the accumulation of lattice distortions. To address this, they designed a simple annealing process to fabricate highly textured (101)-oriented Zn, which

Table 1. Zn Anode Strengthening Strategies and Performances

| Type | Method | Symmetrical cell | | | Reference |
|--------------------------------|---|------------------------------------|---|--------------------------|---------------|
| | | Overpotential | Cycle performance | Electrolyte | |
| Traditional process treatment | Rolling + annealing | 50 mV (10 mA cm ⁻²) | 1050 h (10 mA cm ⁻² , 10 mAh cm ⁻²) | 1 M ZnSO ₄ | ¹⁷ |
| | Mechanical grinding | 47 mV (20 mA cm ⁻²) | 1500 cycle (50 mA cm ⁻² , 1 mAh cm ⁻²) | 2 M Zn(OTf) ₂ | ⁵⁸ |
| | Melting–solidification | 50 mV (10 mA cm ⁻²) | 180 h (10 mA cm ⁻² , 75% DOD) | 2 M ZnSO ₄ | ⁷ |
| | Acid etching | 42.1 mV (0.5 mA cm ⁻²) | 300 h (5 mA cm ⁻² , 5 mAh cm ⁻²) | 3 M Zn(OTf) ₂ | ⁵⁹ |
| | Nitrogen plasma + Thermal radiation | ~50 mV (10 mA cm ⁻²) | 1100 h (10 mA cm ⁻² , 3 mAh cm ⁻²) | 2 M ZnSO ₄ | ⁶⁰ |
| | Annealing | ~45 mV (5 mA cm ⁻²) | 800 h (5 mA cm ⁻² , 1 mAh cm ⁻²) | 2 M ZnSO ₄ | ²⁴ |
| | Rolling + annealing | 47 mV (10 mA cm ⁻²) | 280 h (5 mA cm ⁻² , 5 mAh cm ⁻²) | 2 M ZnSO ₄ | ⁶ |
| | Imprint process | 86.8 mV (10 mA cm ⁻²) | 100 h (10 mA cm ⁻² , 10 mAh cm ⁻²) | 2 M ZnSO ₄ | ⁵⁴ |
| | Acid etching | 27 mV (3 mA cm ⁻²) | 1230 h (3 mA cm ⁻² , 3 mAh cm ⁻²) | 2 M ZnSO ₄ | ⁶¹ |
| | Zn@Ag | 36.5 mV (0.5 mA cm ⁻²) | 630 h (0.5 mA cm ⁻² , 0.5 mAh cm ⁻²) | 1 M ZnSO ₄ | ⁶² |
| Heteroepitaxial growth | MPVMTs | ~40 mV (0.5 mA cm ⁻²) | 2000 h (1 mA cm ⁻² , 1 mAh cm ⁻²) | 2 M ZnSO ₄ | ²⁸ |
| | Act–LDH–H | 39.3 mV (10 mA cm ⁻²) | 420 h (10 mA cm ⁻² , 5 mAh cm ⁻²) | 2 M ZnSO ₄ | ⁶³ |
| | CuZns | ~50 mV (10 mA cm ⁻²) | 90 h (10 mA cm ⁻² , 85% DOD) | 2 M ZnSO ₄ | ³² |
| | Cu(111) | 140 mV (100 mA cm ⁻²) | 30000 cycle (100 mA cm ⁻² , 1 mAh cm ⁻²) | 2 M ZnSO ₄ | ³¹ |
| | MXene | 38 mV (5 mA cm ⁻²) | 145 h (10 mA cm ⁻² , 85% DOD) | 2 M ZnSO ₄ | ³⁹ |
| Functionalized 3D architecture | PVDF–Sn@Zn | 18.9 mV (5 mA cm ⁻²) | 200 h (10 mA cm ⁻² , 10 mAh cm ⁻²) | 2 M ZnSO ₄ | ⁵⁵ |
| | 3D–RFGC@Zn | 72.5 mV (120 mA cm ⁻²) | 2600 h (80 mA cm ⁻² , 80 mAh cm ⁻²) | 2 M ZnSO ₄ | ⁵⁷ |
| | Eutectic Zn ₈₈ Al ₁₂ alloys | 20 mV (0.5 mA cm ⁻²) | 2000 h (0.5 mA cm ⁻²) | 2 M ZnSO ₄ | ⁴⁹ |
| | Thermal infusion 3D skeleton | 44 mV (10 mA cm ⁻²) | 1000 cycle (10 mA cm ⁻² , 1 mAh cm ⁻²) | 2 M ZnSO ₄ | ⁴¹ |
| | 3D ZnOHF nanowire array | ~40 mV (5 mA cm ⁻²) | 400 h (5 mA cm ⁻² , 1 mAh cm ⁻²) | 2 M ZnSO ₄ | ⁵³ |

possesses robust epitaxial growth characteristics (Figure 3d).¹³ Grain boundaries, as a type of defect, exacerbate corrosion and HER due to their enhanced reactivity compared to crystallographic planes.^{25,26} Zhao et al. successfully suppressed side reactions at grain boundaries by preferentially introducing intermetallic compounds into these regions (Figure 3e).²⁷

In addition to Zn metal serving as the substrate, other materials with similar lattice configurations can be employed for the epitaxial growth of Zn. The lattice mismatch, denoted as δ , provides a quantitative measure to evaluate the compatibility between epitaxial crystals and substrate materials (Figure 4a).²⁸

$$\delta = \left| \frac{d_{\text{sub}} - d_{\text{Zn}(200)}}{d_{\text{Zn}(200)}} \right| \quad (3)$$

Drawing from the recognized capillarity of homogeneous nucleation, the solid–solid contact mode within the model of uniform surface deposition can be conceptualized in a manner analogous to the process by which a liquid forms a solid–liquid interface via nucleation on a solid substrate.^{29,30} According to Young's equation:

$$\gamma_{sv} = \gamma_{fs} + \gamma_{fv} \cos \theta \quad (4)$$

where f, s, and v denote the film, substrate, and vapor, respectively. Then γ_{sv} , γ_{fs} , γ_{fv} represent the interface energy between the two phases and θ is the contact angle.

Based on eqs 3 and 4, the deposition behavior of Zn is primarily influenced by the synergistic interaction of two factors: (1) the lattice compatibility between the Zn crystallographic structure and the substrate surface, and (2) the intrinsic interfacial affinity of the Zn metal anode for the

substrate (Figure 4b). Yi et al. introduced a unique dendrite regulation method through facet matching, which fosters the growth of uniformly distributed miniature Zn dendrites with structural homogeneity, thus effectively inhibiting undesirable dendritic coarsening. The periodically exposed Cu (111) facets on copper nanowire ridges aid in dendrite regulation by creating a low lattice-mismatched Zn (002)/Cu (111) interface configuration (Figure 4c).³¹ The MXene membranes, fabricated using the Marangoni effect-driven self-assembly in solution, possess both electrical conductivity and mechanical flexibility, which help in regulating Zn nucleation uniformity and interfacial stress distribution (Figure 4d). Notably, the deposited Zn demonstrates a predominantly (002)-oriented crystallographic texture with high spatial uniformity, achieving an average Coulombic efficiency of 99.67% over 2,400 cycles under 5 mA cm⁻² at 1 mAh cm⁻². Metal ions typically exhibit a natural affinity for their corresponding alloys. By electrocodepositing Zn and Cu onto the Zn electrodes, an interfacial lattice locking layer is created, ensuring stable Zn plating/stripping for over 90 h at an ultrahigh Zn depth of discharge (approximately 85%) (Figure 4e).³² To exploit this characteristic, the construction of Zn-containing alloys or the use of substrates with zincophilic surfaces can effectively enhance uniform ion deposition, such as in the cases of ZnSe, AgZn₃, Zn@Bi, and Zn@Sn.^{32–38}

The primary cause of dendrite's sprawling growth is the planar anode's limited surface area, which readily accumulates excessive local charge and results in an unregulated distribution of Zn²⁺. This discrepancy in the kinetics between Zn²⁺ diffusion and electron transfer rates exacerbates the spatial heterogeneity in ionic distribution. To address this, we propose constructing a 3D high-surface-area anode to slow dendrite

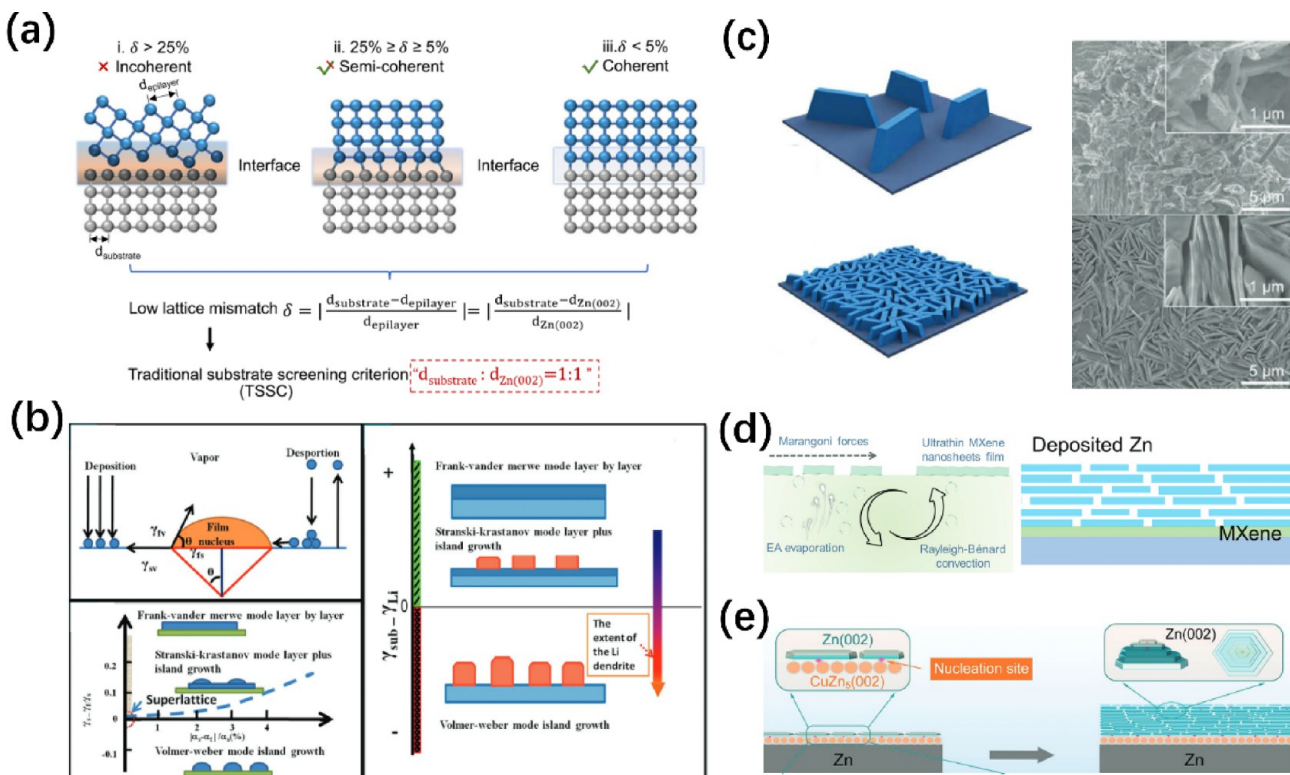


Figure 4. Epitaxial growth of Zn anodes on heterogeneous substrates. (a) Different lattice strain and orientation correlation of Zn electrodeposition formed on substrates.²⁸ Reproduced from ref. 28. (b) The stability regions of the three-film growth modes in coordination of surface energy differences between growing film and growth substrate/lattice misfit.²⁹ Reproduced from ref. 29. (c) A comparison of the Zn and Zn@CuNW anode.³¹ Reproduced from ref. 31. Copyright 2022, John Wiley and Sons Inc. (d) Illustration of the MXene membrane and the corresponding self-assembly mechanism.³⁹ Reproduced from ref. 39. Copyright 2024, John Wiley and Sons Inc. (e) Schematic illustration of the CuZn₅ alloy acting as an ILL layer to regulate the orientation of Zn deposits.³² Reproduced from ref. 32. Copyright 2023, John Wiley and Sons Inc.

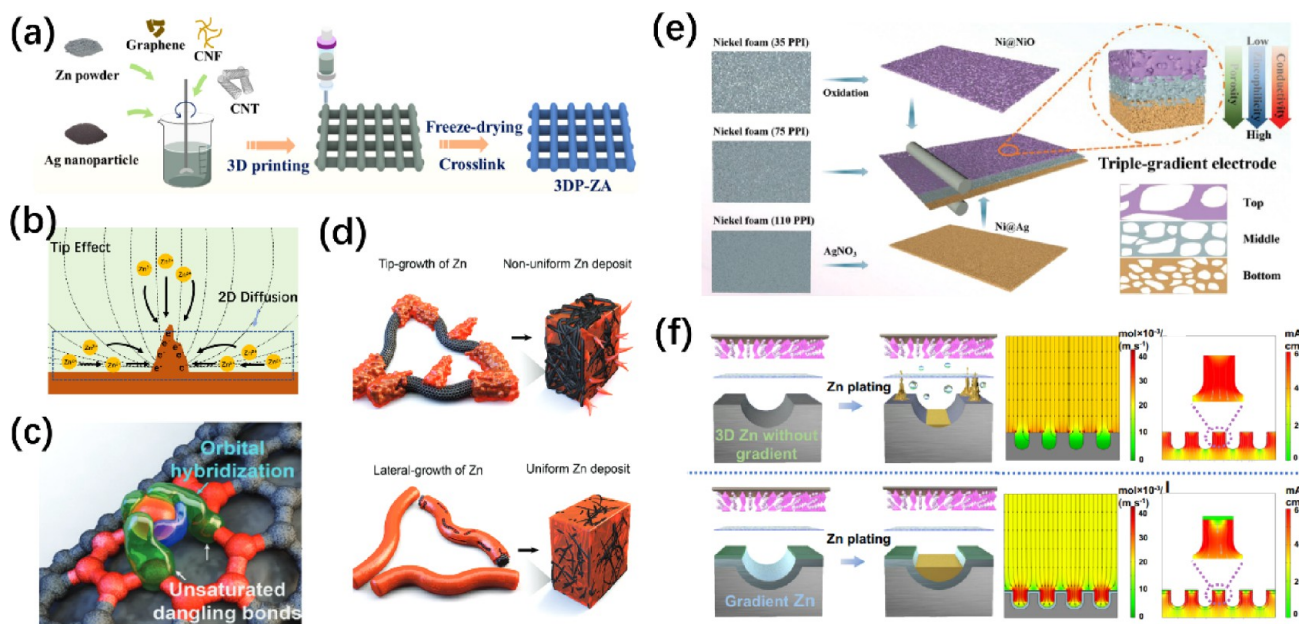


Figure 5. 3D-structured and functionalized Zn anodes. (a) 3D printing technology for Zn anode.⁴² Reproduced with permission from ref. 42. Copyright 2023, Elsevier. (b) Schematic illustration of the 2D diffusion process. (c–d) Schematic illustration of the Zn deposition behavior modulated by carbon nanotube surface defects.⁴⁶ Reproduced with permission from ref. 46. Copyright 2020, Royal Society of Chemistry. (e) Schematic diagram for the triple-gradient electrode fabrication.⁵⁶ Copyright 2022, John Wiley and Sons. (f) Zn deposition behavior and the finite element simulations.⁵⁵ Reproduced from ref. 55.

formation. Nevertheless, directly using foam Zn as an anode is fundamentally flawed due to its structural instability under

repeated cycling, leading inevitably to mechanical degradation and subsequent electrochemical deactivation.⁴⁰ The strategic

choice of electrochemically inert metals, such as copper or carbon nanowire, as scaffold materials for creating 3D conductive architectures proves to offer superior structural integrity. By thermally infusing with a porous Cu (PCu) host, the crafted PCu@Zn anode displays an architecture defined by a dense, planar surface morphology and an integrated CuZn₅ alloy phase.⁴¹ The integration of 3D printing technology allows for precise customization of pore architecture and size distribution in three-dimensional porous structured electrodes.^{12,42} A dendrite-free 3D Ni-Zn anode for aqueous ZIBs is designed and manufactured using 3D printing and further electroless/electro deposition techniques (Figure 5a).⁴³ Featuring a multi-channel lattice structure and super-hydrophilic surface, it effectively improves the electric-field distribution and induces uniform deposition of Zn without dendrite growth.

The tip effect not only introduces spatial heterogeneity in the ion distribution within the electrolyte, but also intensifies and distorts the electric field generated by localized charge accumulation. This drives a two-dimensional diffusion of surface-adsorbed ions toward protrusion sites, leading to the deterioration of dendrites (Figure 5b).^{44–48} It has been reported that on defect-free carbon felt electrodes, the surface diffusion of Zn adatoms/nuclei propels Zn aggregation and initiates Zn deposition on the tip part of the carbon fibers, creating a nonuniform Zn deposition morphology. Conversely, single vacancy defects facilitate Zn-sp² carbon orbital hybridization through unsaturated bonds, which inhibit Zn aggregation by stabilizing early-stage electrodeposition (Figure 5c,d).⁴⁹

In addition to the ex situ fabrication of three-dimensional anode architectures, another promising approach is the use of eutectic alloying strategies. By introducing a secondary phase into the anode matrix, this method provides structural scaffolding that enhances cycling stability.³⁰ Notably, the eutectic alloying of Zn and aluminum has been shown to effectively address the challenges associated with Zn reversibility. This technique employs a lamellar nanostructure characterized by alternating Zn and Al nanolamellae (Zn₈₈Al₁₂, at.%). Within this alloy, the protective Al lamellae not only shield the Zn lamellae, creating an irreversible product, but they also in situ form stable Al/Al₂O₃ interlamellar structures. These structures subsequently guide the growth of Zn while suppressing the tip effect.⁴⁹ Moreover, analogous research indicates that variations in the stoichiometric ratio for Zn-Al alloys lead to different Zn deposition behaviors, which can be modulated through the electrostatic shield.⁵⁰

Zn deposition on heterogeneous supports requires overcoming the nucleation energy barrier, which is linked to the binding energy of the support materials with the Zn atom. The zincophilicity of these supports is vital for regulating Zn²⁺ plating. Conversely, zincophobia can be employed to restrict undesired Zn deposition.⁵¹ The combination of zincophilic/zincophobic properties with three-dimensional architectures, along with precise control of fabrication processes, facilitates the creation of lithium-free anodes that display multiscale gradient structures and multifunctional characteristics.^{52–57} A triple-gradient electrode is designed with incrementally enhanced conductivity, zincophilicity, and porosity from the surface to its core. This contributes to a higher Zn²⁺ ion flux, optimized local charge-transport dynamics, and the preferred bottom-up deposition behavior for Zn metals (Figure 5e).⁵⁶ Using the imprinting and coating process, the PVDF-Sn@Zn

gradient electrode is produced (Figure 5f).⁵⁵ The hydrophobic nature of the PVDF layer, combined with the high redox potential of Sn (Sn²⁺/Sn, -0.136 V vs SHE), effectively safeguards Zn metal from corrosion in the electrolyte. Moreover, the gradient conductivity efficiently directs electric field distribution, Zn²⁺ ion flux, and local current density toward the base of the microchannels, thus achieving the desired bottom-up deposition behavior for Zn metal.

3.2. Zn Anode Protective Layer. While Zn metal anodes demonstrate high specific capacity during charge and discharge processes, their limited reversibility in these electrochemical reactions poses significant constraints to long-term energy storage. Notably, most research to date has predominantly centered on the degradation of performance due to cycling, overlooking the profound impact of calendar aging on Zn metal behavior. Unlike lithium-ion chemistry, Zn anodes lack a self-limiting solid electrolyte interphase (SEI), resulting in markedly distinct aging dynamics: a linear temporal scaling of capacity loss, influenced by interfacial reaction kinetics, as opposed to the parabolic time dependence observed in LIBs which is governed by Fickian diffusion. This difference stems from the inherent susceptibility of the Zn electrode to corrosion during storage. In this context, unregulated electrolyte decomposition leads to the formation of porous passivation products, rather than protective films, ensuring continued consumption of active material and precipitating accelerated failure modes (Figure 6a,b).⁶⁴

The majority of adverse reactions occur at the interface between the anode and electrolyte, necessitating the creation of an effective protective layer. This layer acts as a buffer zone, physically separating the anode and electrolyte to inhibit potential side reactions. Such protective layers take on a variety of configurations, with this review focusing on the SEI and artificial SEI (ASEI), as shown in Table 2. The SEI is typically formed in situ via spontaneous reactions between the anode and electrolyte components at the electrode surface, while the ASEI is artificially constructed through presynthesis. Generally, when exposed to air and moisture, Zn metal forms a dense layer of Zn₅(CO₃)₂(OH)₆, which can transform into an interphase of Zn₄SO₄(OH)₆·xH₂O (ZHS) in mild acid electrolytes.⁶⁶ However, this loose compound exacerbates dendrite growth and reduces Coulombic efficiency for Zn stripping/plating, rather than protecting the Zn anode from ongoing corrosion. To mitigate this issue, the use of additives can lower the surface energy, encouraging the growth of horizontally dense ZHS nanosheets (Figure 6c).^{65,67}

The process of ZHS formation typically involves a reaction with water, which is marked by the evolution of hydrogen gas. Enhancements to this process can be made via the addition of ZnF₂^{68–72} or Zn₃(PO₄)₂^{10,73–76} additives, which help to construct the SEI layer. This not only effectively curbs parasitic reactions and dendritic growth but also facilitates rapid ion migration rates. The integration of 40 vol % tetramethylurea (TMP) into the electrolyte successfully adjusts the solvation sheath of Zn²⁺ ions, creating a gradient-structured ZnF₂-Zn₃(PO₄)₂ SEI layer on the surface. This is achieved owing to the distinct chemical reactivity between TMP and OTf⁻ anions, which allows for stable battery operation at -50 °C by suppressing parasitic reactions and optimizing ion transport kinetics (Figure 7a).⁷⁷ A combination of theoretical calculations and experimental characterizations reveals that the outer ZnF₂ layer primarily eases Zn²⁺ desolvation, while the inner Zn₃(PO₄)₂ domain forms swift ion transport pathways

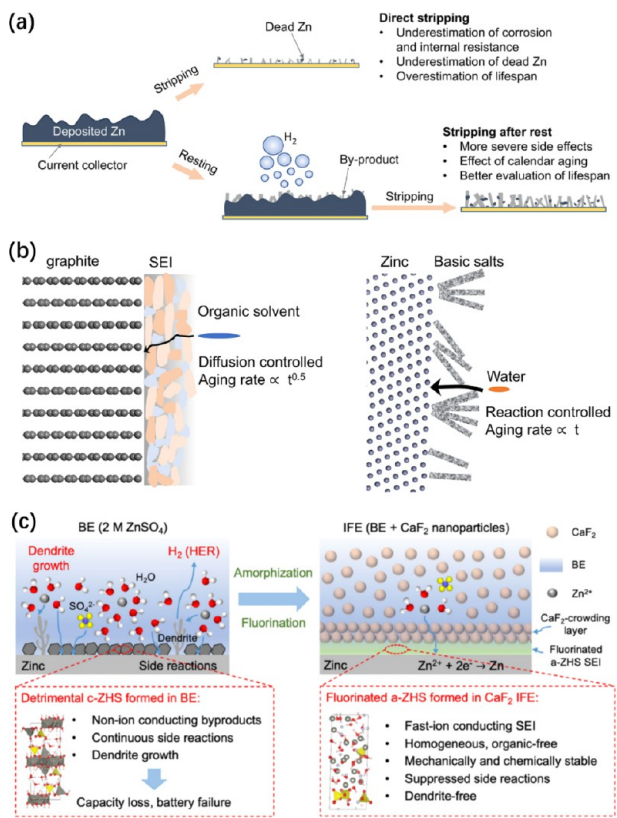


Figure 6. Importance and impact of SEI on Zn anodes. (a) Major factors and consequences of calendar aging in Zn metal anodes.⁶⁴ (b) Schematic of the calendar aging mode.⁶⁴ Reproduced with permission from ref. 64. Copyright 2024, Elsevier. (c) Comparative schematic illustration: corrosion degradation of bare substrate (left) vs CaF₂-protected interfacial layer (right).⁶⁵ Reproduced from ref. 65. Copyright 2025, American Chemical Society.

for Zn species (Figure 7b). This hierarchical structure establishes a synergistic mechanism that addresses desolvation energy barriers and ionic conductivity needs under cryogenic conditions. Recent research has shown that PPS additives, with their dual adsorption sites, effectively reconfigure the hydrogen-bond network in electrolytes and form a dynamic electrochemical double layer (EDL). In tandem, the *in situ* decomposition of PPS generates a self-healing SEI layer, enabling an impressive cycling stability of 500 h under a current density of 50 mA cm⁻², with a depth of discharge of 42.7% (Figure 7c).⁷⁸

The *in situ* formation of SEI inherently activates complex chemical processes, such as solvent decomposition, hydrolysis reactions, cross-linking of organic molecules, and oxidative passivation (Figure 7d).⁷⁹ While this suggests a degree of self-healing capability, it also results in poorly controlled compositional gradients and heterogeneous physicochemical properties (Figure 7e).⁸⁰ These intrinsic limitations significantly impede the practical application of naturally formed SEI layers. In contrast, ASEI engineered through precise process design, offer superior controllability and structural homogeneity.

In 2020, a robust and homogeneous ZnS interphase was developed on the Zn surface through a vapor–solid strategy. The thickness of this interphase can be modulated by adjusting the treatment temperature (Figure 8a).⁶⁶ To enhance ionic transport, zincophilic coatings were introduced to decrease the

interfacial energy barrier for nucleation. Examples of such coatings include ZnTe,⁸¹ ZnSe³⁴ or ZnP⁸² interlayers, which notably accelerate the Zn redox kinetics. As an advanced approach to bolster the SEI's performance, the incorporation of a multi-layered architecture has been suggested, aiming for multi-functionalization. A coupling strategy consists of a VSe₂-ZnSe hybrid outer layer with minimal lattice mismatch and exceptional electronic conductivity, fostering organized planar Zn growth. Simultaneously, the nanometallic inner V layer exhibits outstanding corrosion resistance, counteracting electrolyte degradation of the anode (Figure 8b).⁸³ Drawing inspiration from the biological structure of lotus leaves, Zhang et al. proposed a sandwich-structured SEI film that offers versatile properties, achieved through three distinct fabrication techniques (Figure 8c).⁸⁴ The first layer is a self-assembled monomolecular layer created by triethoxy-3-aminopropylsilane. The second layer is a highly flexible one formed by polydimethylsiloxane (PDMS). The third layer is a superhydrophobic one, formed by an amalgamation of trimethoxy(octadecyl)silane (OTS)-modified nanosilicon dioxide (SiO₂) and PDMS. A superhydrophobic layer with a micro-nano composite rough structure is fabricated by spraying SiO₂-OTS particles on the PDMS surface. This layer repels free water molecules in the electrolyte, thereby inhibiting corrosion on the Zn anode effectively. In order to optimize Zn²⁺ plating kinetics and establish a more stable SEI, we construct a self-assembly of triethoxy-3-aminopropylsilane on the Zn anode *in situ* using the typical soaking method. The intermediate PDMS layer serves two purposes; it provides a substrate for surface-anchored SiO₂-OTS nanoparticles and allows usage in flexible device technologies due to its flexibility. Apart from these systems, materials with channel-like or layered architectures such as graphene,⁸⁵ MXenes,⁸⁶ and metal–organic frameworks (MOFs)^{87–89} have also shown considerable potential for SEI (Figure 8d–f).

There are several key factors that should be considered when designing high-performance SEI. (i) In SEIs, ion transport often serves as the rate-determining step for the overall electrochemical kinetics of full-cell systems.⁹⁰ Consequently, the SEI should be composed of materials with a high density of ion nanochannels. These nanochannels must allow rapid Zn²⁺ diffusion and function as molecular sieves to exclude water molecules, thereby preventing direct anode–electrolyte decomposition reactions. Additionally, a low interface impedance and quick kinetics are essential to ensure high discharge/charge rates in the batteries. (ii) The SEI performs its primary protective role through two crucial mechanisms: it physically decouples the anode from the bulk electrolyte to eliminate direct electrochemical contact, and it suppresses parasitic electron tunneling across the interface, which would drive harmful side reactions between reactive electrode surfaces and electrolyte species. Therefore, the SEI must maintain high ionic conductivity while exhibiting negligible electronic conductivity. Under high current density, any significant electronic conduction could allow electrons to percolate through the SEI, leading to uncontrolled Zn deposition via direct surface reduction.^{39,91} This mechanism would compromise the SEI's protective ability, leading to dendrite proliferation and recrudescence of electrolyte decomposition side reactions (Figure 9a). (iii) Zincophilic and zincophobic properties are key design parameters that control the behavior of Zn²⁺ deposition. Materials with a

Table 2. Zn Anode Solid–Electrolyte Interphase and Performance

| Type | Method | Thickness | Symmetrical cell cycle performance | Full Cell | | Reference |
|---|--|--|--|---|--|--|
| | | | | Anode/ Cathode | Cycle performance | |
| In situ SEI | Zn (BF_4) ₂ –DMSO a-ZHS | 21 ~ 24 nm ~30 nm | 5750 h (1 mA cm ⁻² , 1 mAh cm ⁻²) 1000 h (–) | Zn PANI | 600 cycles (0.1 A g ⁻¹) | Zn(BF_4) ₂ + DMSO 70 |
| | Zn ₃ (PO ₄) ₂ | – | 1800 h (3 mA cm ⁻² , 1 mAh cm ⁻²) | Zn INVO | 20000 cycles (3 A g ⁻¹) | 2 M ZnSO ₄ + CaF ₂ 65 |
| Bilayer/P–F | 35 nm | 120 h (40 mA cm ⁻² , 40 mAh cm ⁻²) | Zn CVO | 1000 cycles (5 A g ⁻¹) | 2 M ZnSO ₄ + β -GP 75 | |
| γ -GVL | – | 2300 h (–40 °C, 0.2 mA cm ⁻² , 0.2 mAh cm ⁻²) | Zn NaVO | 200 cycles (3 A g ⁻¹) | 2 M Zn(OTf) ₂ + 20 mM aniline 69 | |
| ZSO/TCB | – | 1200 h (1 mA cm ⁻² , 1 mAh cm ⁻²) | Zn VO ₂ | 300 cycles (–20 °C, 0.5C) | 2 M Zn(OTf) ₂ + 20 vol % γ -GVL 68 | |
| PRS | ~30 nm | 540 h (50 mA cm ⁻² , 5 mAh cm ⁻²) | Zn I ₂ | 3400 cycles (1 A g ⁻¹) | 2 M ZnSO ₄ + 20 mM TCB 45 | |
| Zn(OTf) ₂ /CLE | 10 μm | 800 h (5 mA cm ⁻² , 2 mAh cm ⁻²) | Zn INVO | 10000 cycles (3 A g ⁻¹) | 2 M ZnSO ₄ + 0.05 M PPS 78 | |
| GPC | – | 1450 h (1 mA cm ⁻² , 4 mAh cm ⁻²) | Zn MnO ₂ | 3000 cycles (2 A g ⁻¹) | 1 M Zn(OTf) ₂ + 2.0 wt % CLE 48 | |
| DMTFA | 31 nm | 4000 h (20 mA cm ⁻² , 20 mAh cm ⁻²) | Zn VS ₂ | 220 cycles (0.5 A g ⁻¹) | 1 M ZnSO ₄ + 4 M GPC 76 | |
| LACA | – | 2000 h (–40 °C, 0.25 mA cm ⁻² , 0.25 mAh cm ⁻²) | Zn INVO | 11000 cycles (1 A g ⁻¹) | 1.2 M Zn(OTf) ₂ in H ₂ O/DMF/DMTFA 110 | |
| ZnF ₂ –Zn ₃ (PO ₄) ₂ | – | 7000 h (–50 °C, 0.4 mA cm ⁻² , 0.4 mAh cm ⁻²) | Zn PANI | 8000 cycles (–40 °C, 0.5 A g ⁻¹) | 1 M Zn(BF_4) ₂ in THF/H ₂ O 72 | |
| DMMF | 300 nm | 4750 h (1 mA cm ⁻² , –) | Zn KVOH | 12000 cycles (–50 °C, 0.5 A g ⁻¹) | 2 M Zn(OTf) ₂ + 40 vol % TMP 77 | |
| PT–ZHC–Sn | ~20 μm | 6500 h (0.5 mA cm ⁻² , 0.5 mAh cm ⁻²) | Zn V ₂ O ₅ | 4000 cycles (5 A g ⁻¹) | 0.5 M Zn(OTf) ₂ in DMMP/H ₂ O 73 | |
| FAP | 8–10 μm | 1000 h (2 mA cm ⁻² , 1 mAh cm ⁻²) | Zn MnO ₂ | 1000 cycles (2 A g ⁻¹) | PDDA-TFSI 92 | |
| Artificial SEI | [PVIPS][Zn(TFSI) ₂]@Zn | 67 μm | 1950 h (1 mA cm ⁻² , 1 mAh cm ⁻²) | Zn HVO | 800 cycles (3 A g ⁻¹) | 2 M ZnSO ₄ 44 |
| MOF–E | 4 μm | 900 h (0.2 mA cm ⁻² , 2 mAh cm ⁻²) | Zn PANI | 2000 cycles (0.5 A g ⁻¹) | 2 M ZnSO ₄ 94 | |
| ZnTe | 1.2 μm | 3000 h (1 mA cm ⁻² , 1 mAh cm ⁻²) | Zn KVOH | 5000 cycles (8 A g ⁻¹) | 2 M ZnSO ₄ 87 | |
| AG–PAM gel | 30 μm | 3500 h (1 mA cm ⁻² , 1 mAh cm ⁻²) | Zn C | 1000 cycles (2 A g ⁻¹) | 2 M ZnSO ₄ 108 | |
| VZSe/N@Zn | – | 650 h (20 mA cm ⁻² , 10 mAh cm ⁻² , 68.4% DOD) | Zn ZMVVO | 250 cycles (1 A g ⁻¹) | 2 M ZnSO ₄ 83 | |
| SFM/Zn | 10 μm | 1800 h (1 mA cm ⁻² , 1 mAh cm ⁻²) | Zn INVO | 3000 cycles (5 A g ⁻¹) | 2 M ZnSO ₄ 84 | |
| ZP@Zn | 20 μm | 1800 h (10 mA cm ⁻² , 1 mAh cm ⁻²) | Zn VO ₂ | 1000 cycles (2 A g ⁻¹) | 2 M ZnSO ₄ 111 | |

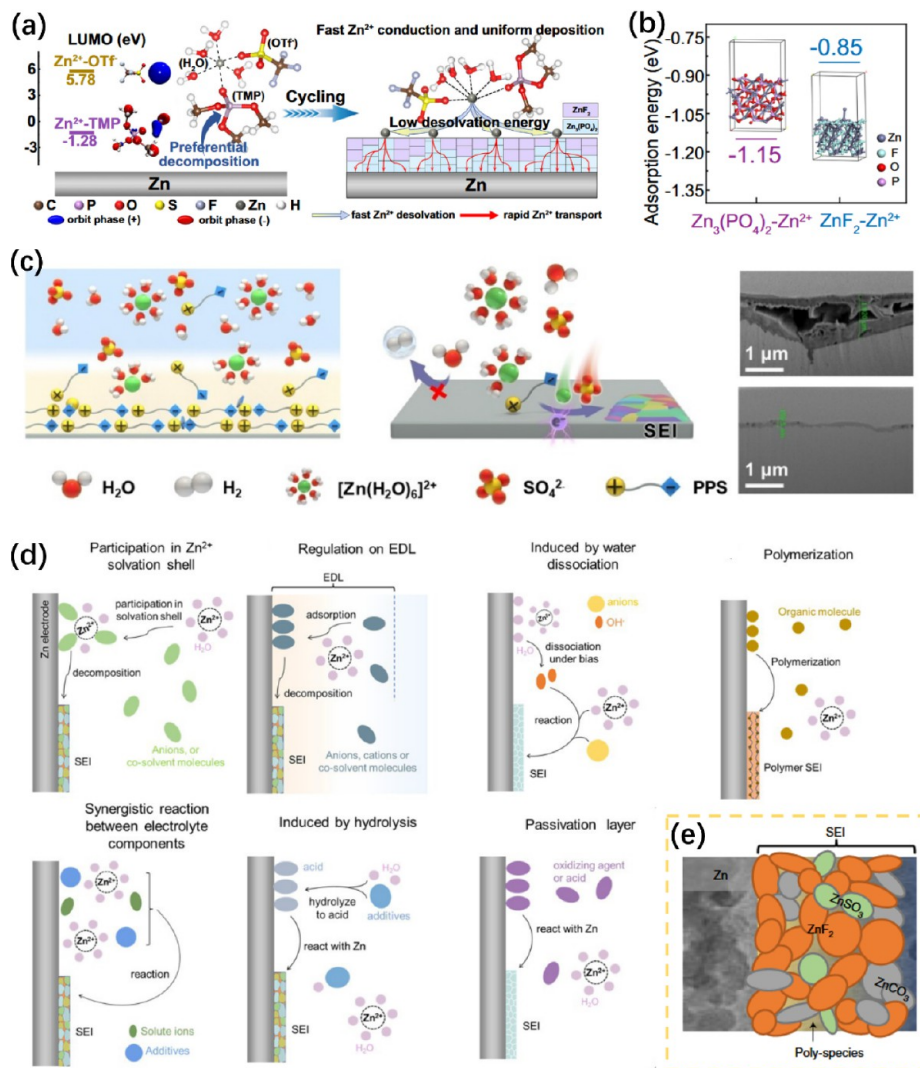


Figure 7. In situ formed SEI membranes on Zn anodes and the mechanisms. (a)–(b) Schematic illustration of the formation process and action mechanism of $\text{ZnF}_2\text{-Zn}_3(\text{PO}_4)_2$ interlayer.⁷⁷ Reproduced from ref. 77. (c) Schematic illustration of the self-repairing SEI.⁷⁸ Reproduced with permission from ref. 78. Copyright 2024, John Wiley and Sons Inc. (d) Schematic diagram of the SEI formation mechanism.⁷⁹ Reproduced with permission from ref. 79. Copyright 2023, John Wiley and Sons Inc. (e) Schematic diagram illustrating the complex composition of the SEI.⁸⁰ Reproduced with permission from ref. 80. Copyright 2021, Springer Nature.

higher absolute value than Zn have stronger Zn bonding ability (zincophilic), which tends to lower the energy of Zn nucleation and make the subsequent deposition more uniform. On the other hand, materials with a smaller absolute value have weaker Zn bonding ability (zincophobic) and can regulate the structures of Zn^{2+} solvation, thereby preventing harmful reactions (Figure 9b).⁵¹ A balance must be struck between “zincophilic” and “zincophobic” properties to leverage their respective strengths. One promising design strategy is to engineer multilamellar SEI architectures with varying functionalities. The layer connected to the anode should have tailored zincophilicity to encourage rapid Zn^{2+} surface diffusion and epitaxial plating, while the layer facing the electrolyte should have zincophobic characteristics to enforce desolvation activation energy thresholds and slow down hydrogen evolution reaction kinetics (Figures 9c and 8f).^{51,84,92–94} (iv) The SEI must maintain its chemo-mechanical stability in electrolyte environments (Figure 9d), demonstrating both electrochemical passivity and sufficient fracture toughness to

resist mechanical stress caused by volume changes during Zn deposition/dissolution cycles.

Conventionally, inorganic SEIs exhibit higher Young's modulus, making them less susceptible to dendrite penetration. Materials with layered structures, such as kaolin,^{95,96} are often preferred due to their propensity for facilitating rapid ionic transport pathways. However, their inherent brittleness and poor contact with Zn anodes result in delamination or fragmentation of SEIs under high DOD cycling, leading to compromised performance. Additionally, some inorganic coatings with micron-scale pore structures lack sufficient electrolyte isolation,^{97,98} rendering them more analogous to functional separators rather than strict SEIs. Comparatively, polymer-based SEI membranes demonstrate superior mechanical resilience and contact stability under complex stress conditions because of their flexible polymer chain structures.⁹⁹ Their strong binding interactions with Zn ions, which can be achieved through the use of polymers inherently rich in polar functional groups or via intentional design of such functionalities into the SEI framework, further lead to significantly

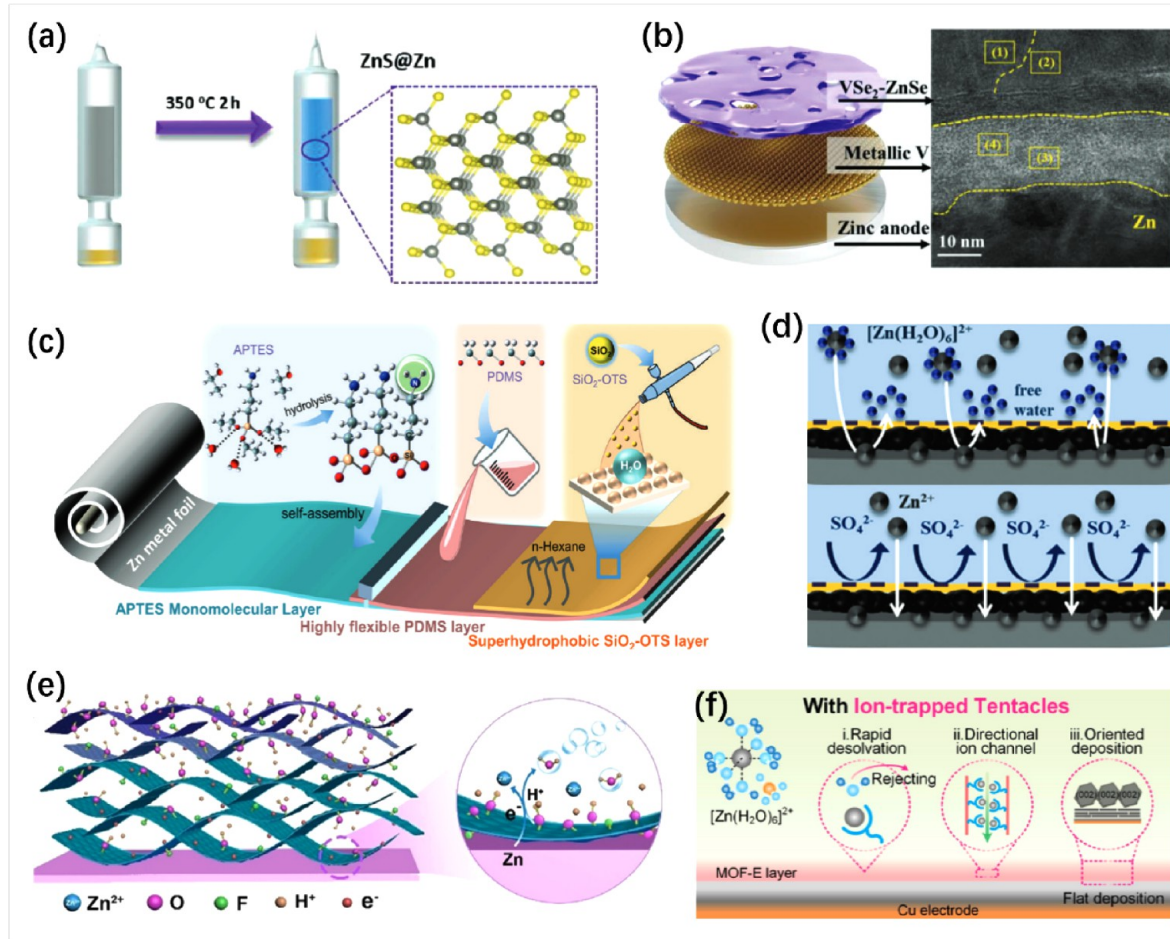


Figure 8. Various types of artificial interfacial layers on Zn anodes. (a) The ZnS solid–electrolyte interphase.⁶⁶ Reproduced with permission from ref. 66. Copyright 2020, John Wiley and Sons Inc. (b) The VSe_2 - ZnSe solid–electrolyte interphase.⁸³ Reproduced with permission from ref. 83. Copyright 2024, John Wiley and Sons Inc. (c) Schematic diagram of the ASEI layer on Zn anode surface.⁸⁴ Reproduced with permission from ref. 84. Copyright 2024, John Wiley and Sons Inc. (d) Schematic diagram of the desolvation and deionization interface layer.⁸⁵ Reproduced with permission from ref. 85. Copyright 2021, Royal Society of Chemistry. (e) The MXene material for constructing the SEI.⁸⁶ Reproduced with permission from ref 86 Copyright 2020, John Wiley and Sons Inc. (f) The MOF material for constructing the SEI.⁸⁷ Reproduced with permission from ref 87 Copyright 2023, John Wiley and Sons Inc.

enhanced ionic conductivity.^{100–103} However, polymer-based SEI in aqueous electrolytes remain limited in ionic conductivity, which results in significant polarization overpotential. The creation of inorganic–organic composites, through synergistic integration of both components, generates abundant interfacial regions between inorganic and organic matrices.¹⁰⁴ These interfaces enhance ionic diffusion kinetics and effectively combine the mechanical flexibility of polymer frameworks with the structural stability of inorganic SEI materials for improved electrochemical performance^{105,106} (Figure 9e).

In light of the previously discussed characteristics, it is clear that the SEI shares attributes with solid-state electrolytes, notably high ionic conductivity and low electronic conductivity. The evolution of SEI might benefit from insights gleaned from advancements in solid-state electrolyte technologies, even though contemporary solid-state electrolytes face obstacles such as suboptimal ion transport kinetics and insufficient interfacial compatibility. Rather than pursuing complete water isolation, the use of hydrogel-based confinement strategies offer a viable alternative. These approaches can effectively restrict the movement of active water species, thus

reducing unwanted interfacial reactions. Concurrently, they enhance interfacial compatibility and expedite ionic transport kinetics (Figure 9g).

3.3. Electrolyte Optimization. As a crucial component of AZIBs, aqueous electrolytes are primarily known for their low cost, high safety, good ion conductivity, and environmental friendliness. These properties also determine the electrochemically stable potential and the reversibility of the Zn plating/stripping process. The duality of Zn, which allows Zn^{2+} to react with both OH^- and H^+ , can promote corrosion or the formation of by-products. Consequently, highly acidic or alkaline electrolytes are unsustainable. However, in a mildly acidic environment, the formation of by-products is effectively mitigated due to the presence of a small amount of H^+ . Therefore, neutral or mildly acidic aqueous electrolytes are more commonly used in AZIBs. Generally, the type of anion species largely determines the physicochemical properties of the electrolytes, including ionic conductivity, viscosity, and electrochemical stability.^{112,113} For instance, the $\text{Zn}(\text{ClO}_4)_2$ solution exhibits a high overpotential due to the formation of a passivation layer from its strong oxidizing properties, while ZnNO_3 exacerbates anode erosion.¹¹⁴ In contrast, organic

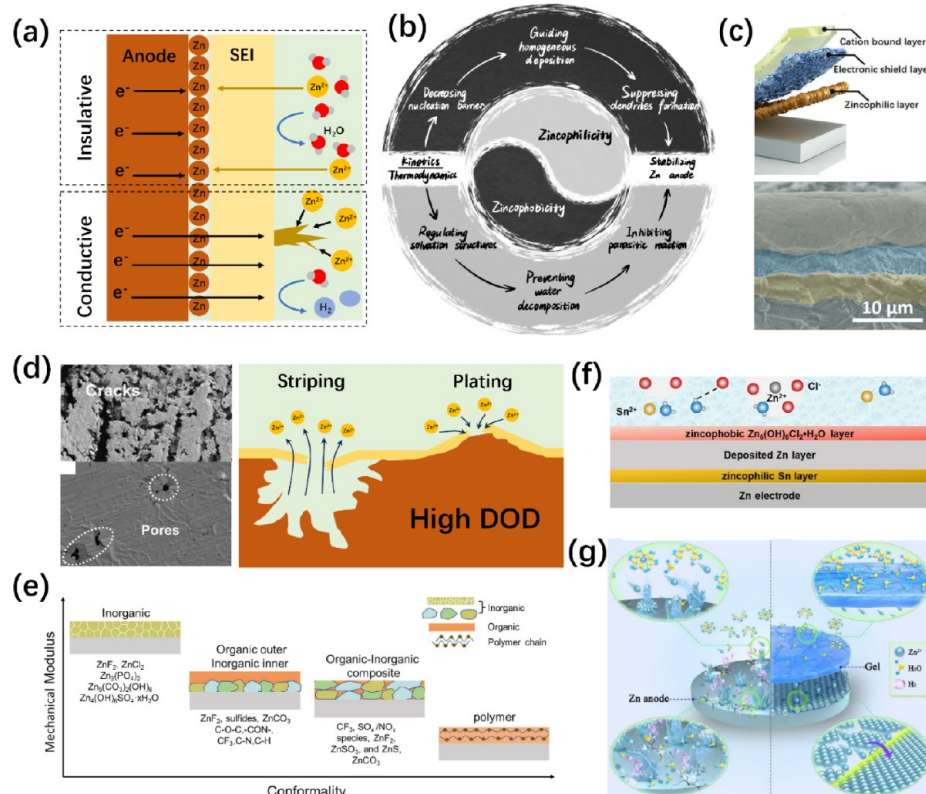


Figure 9. Characteristics of SEI layers on Zn anodes. (a) Schematic diagram of the insulative/conductive SEI. (b) Correlation between zincophilicity and zincophobicity in the Zn metal anode.⁵¹ Reproduced from ref 51. (c) The in situ self-reconstructed triple-gradient layer.⁹² Reproduced with permission from ref. 92. Copyright 2024, John Wiley and Sons Inc. (d) Schematic diagram of SEI damage caused by the volume change at high DOD during cycling.¹⁰⁷ Reproduced with permission from ref. 107. Copyright 2024, Royal Society of Chemistry. (e) Mechanical characteristics of different types of SEI.⁷⁹ Reproduced with permission from ref. 79. Copyright 2023, John Wiley and Sons Inc. (f) Schematic of the electrolyte–electrode–interphase structures of zincophilic–zincophobic interfacial layers.⁹³ Reproduced with permission from ref. 93. Copyright 2021, John Wiley and Sons Inc. (g) Hydrogel materials are used for constructing SEI.¹⁰⁸ Reproduced with permission from ref. 108. Copyright 2023, Elsevier.

electrolytes offer a wider voltage window and better stability. The bulky organic anion (e.g., CF_3SO_3^- , TFSI^- , CH_3COO^-) with a larger radius can disrupt the solvation structure of hydrated cations, reduce the water molecules surrounding Zn^{2+} , and thereby decrease the energy barrier required for desolvation.

The study of ion solvation shells and hydrogen bond networks in solutions has garnered significant attention, as strategies for electrolyte optimization primarily focus on adjusting their structural hierarchies and intermolecular interactions. Within these mechanistic frameworks, aqueous eutectic electrolytes (AEEs) have been proposed. These electrolytes contain three or more components, characterized by at least one hydrogen bond donor paired with a hydrogen bond acceptor.^{115,116} The formulation of these aqueous eutectic electrolytes is complex, governed by the interplay of intermolecular forces including hydrogen bonding, Lewis acid–base interactions, and van der Waals attractions (Figure 10a).^{117,118} The formation of continuous hydrogen-bonded networks significantly lowers the melting point of the electrolyte system and reduces water activity, which in turn suppresses water decomposition and enhances ionic conductivity.¹¹⁹ A specifically designed dual salt/dual solvent electrolyte ($\text{Zn}(\text{BF}_4)_2/\text{Zn}(\text{Ac})_2$ in water/TEGDME) effectively inhibits Zn corrosion through the TEGDME ether cosolvent. This is achieved by reducing water activity at the

outer Zn ion solvation structure, resulting in a high Coulombic efficiency of 99.80% at a deep Zn anode discharge of 60% (Figure 10c).¹²⁰

In dilute electrolyte solutions, ionic conductivity typically rises with increasing concentration. However, beyond a certain point, the ionic conductivity starts to decline, and there are significant changes in properties like the electrochemical window, viscosity, density, and other related characteristics.¹²¹ This method, known as the “water-in-salt electrolyte” (WISE), was initially introduced by Suo et al. in 2015.¹²² When salt concentration reaches an ultrahigh level, the electrostatic field produced by the abundant cationic charges is not fully neutralized by the limited water molecules, which results in anions being drawn into solvation sheaths. This process intensifies cation–anion interactions, reduces water activity, significantly expands the electrochemical window, and simultaneously inhibits side reactions (Figure 10d).¹²³ Beyond merely elevating the electrolyte concentration, the incorporation of concentrated supporting salts provides an alternative approach to achieve comparable electrochemical performance.^{124–126} Conventional approaches employing this strategy often necessitate large quantities of expensive and environmentally harmful salts.¹²⁷ In contrast, Dong et al. cleverly utilize hydroscopic solubilization to dissolve the otherwise low-solubility yet cost-effective and eco-friendly zinc acetate electrolyte to an unexpectedly high concentration of 23 M,

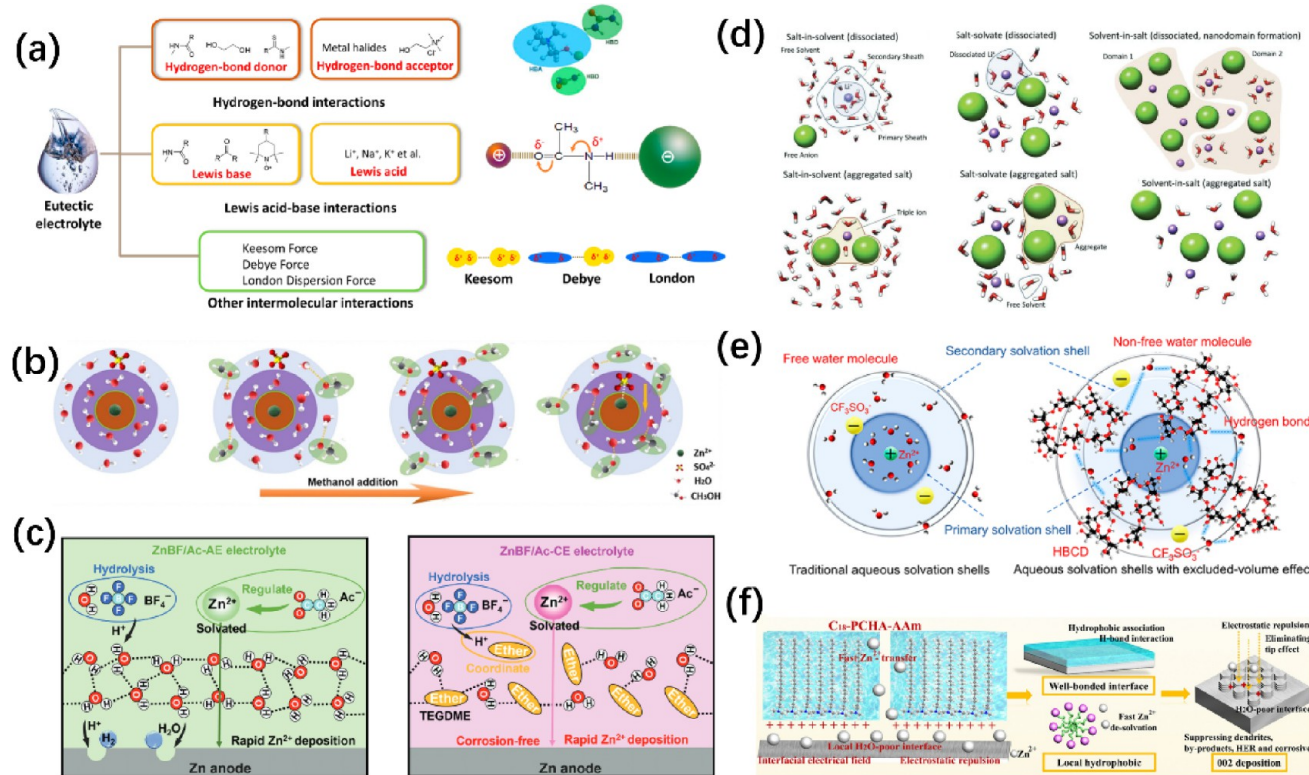


Figure 10. Working mechanisms of eutectic electrolyte, water-in-salt electrolyte, molecularly crowded electrolytes, and hydrogel electrolytes. (a) Formation mechanisms of eutectic electrolytes.¹¹⁷ Reproduced from ref. 117. Copyright 2020, American Chemical Society (b) Schematic of the changes in the Zn²⁺ solvent sheath.¹³³ Reproduced with permission from ref. 133. Copyright 2021, John Wiley and Sons Inc. (c) Schematics of the Zn anode interfacial reactions in ZnBF₄/Ac-AE and ZnBF₄/Ac-CE electrolytes.¹²⁰ Reproduced with permission from ref. 120. Copyright 2024, John Wiley and Sons Inc. (d) The dissociation and aggregation process of salts in WISE.¹²¹ Reproduced with permission from ref. 121. Copyright 2023, John Wiley and Sons Inc. (e) Schematic illustration of the Zn²⁺ solvation shells in traditional aqueous electrolytes and HBCD excluded-volume electrolytes.¹³¹ Reproduced with permission from ref. 131. Copyright 2022, American Chemical Society (f) Schematic of the amphiphilic polycation hydrogel electrolyte.¹³² Reproduced with permission from ref. 132. Copyright 2024, Royal Society of Chemistry.

Table 3. Performance Comparisons of AEEs, WISEs, MCW, and HGEs

| Type | Electrolyte | Anode cathode | Cycle performance | Reference |
|------|---|--------------------------------------|---|-----------|
| SAEE | Zn(BF ₄) ₂ /Zn(Ac) ₂ in H ₂ O/TEGDME | Zn PANI | 400 cycles (5 mA cm ⁻²) | 120 |
| | Zn(BF ₄) ₂ in H ₂ O/Acetamide | Zn PANI | 8000 cycles (5 A g ⁻¹) | 134 |
| | Zn(OTf) ₂ + H ₂ O/Acetamide/Caprolactam | Zn VS ₂ | 800 cycles (0.5 A g ⁻¹) | 135 |
| | Zn(OTf) ₂ + H ₂ O/EG | Zn NVO | 600 cycles (1 A g ⁻¹) | 136 |
| | Zn(OTf) ₂ + H ₂ O/TMS | Zn NVO | 200 cycles (0.2 A g ⁻¹) | 137 |
| | Zn(ClO ₄) ₂ /InCl ₃ + H ₂ O/EG | Zn PANI | 2000 cycles (3 A g ⁻¹) | 138 |
| WISE | 20 M LiTFSI + 1.0 M Zn(TFSI) ₂ | Zn LiMn ₂ O ₄ | 4000 cycles (4 C) | 139 |
| | 20 M LiTFSI + 1.0 M Zn(OTf) ₂ | Zn LiMn ₂ O ₄ | 300 cycles (5 C) | 140 |
| | 10 M Zn(Ac) ₂ | Zn PTO | 1200 cycles (10 C) | 128 |
| | 20 M ZnCl ₂ + 5.0 KI | Zn rGO-I ₂ | 1200 cycles (20 mA cm ⁻²) | 141 |
| | 30 M ZnCl ₂ | Zn WO ₃ | 1000 cycles (1 A g ⁻¹) | 142 |
| MCE | Zn(OTf) ₂ + H ₂ O/HBCD | Zn DC-PDESA | 2000 cycles (10 C) | 131 |
| | Zn(OTf) ₂ + H ₂ O/Sulfolane | Zn ZVO | 350 cycles (0.5 C) | 143 |
| | ZnSO ₄ +H ₂ O/Betaine | Zn VO ₂ | 170 cycles (2 A g ⁻¹ , -30 °C) | 144 |
| | Zn(OTf) ₂ + H ₂ O/PEG | Zn V ₂ O ₅ | 1600 cycles (2 A g ⁻¹) | 145 |
| | Zn(TFSI) ₂ /LiTFSI + H ₂ O/PEG | Zn LFP | 200 cycles (0.2 C) | 146 |
| | Zn(OTf) ₂ /ZnBr ₂ + H ₂ O/PEG | Zn AC | 5000 cycles (5 A g ⁻¹) | 147 |
| HGE | Fe ³⁺ -PAA/CNF | Zn PANI | 200 cycles (1 A g ⁻¹ , -30 °C) | 148 |
| | BBAS | Zn I ₂ | 5000 cycles (5 C, -50 °C) | 149 |
| | PAHE | Zn LFP | 300 cycles (1 C) | 150 |
| | SA | Zn MnO ₂ | 1500 cycles (6 C) | 151 |
| | DCZ-gel | Zn PANI | 2000 cycles (2 A g ⁻¹) | 152 |
| | PDHE | Zn MnO ₂ | 200 cycles (0.2 A g ⁻¹) | 153 |

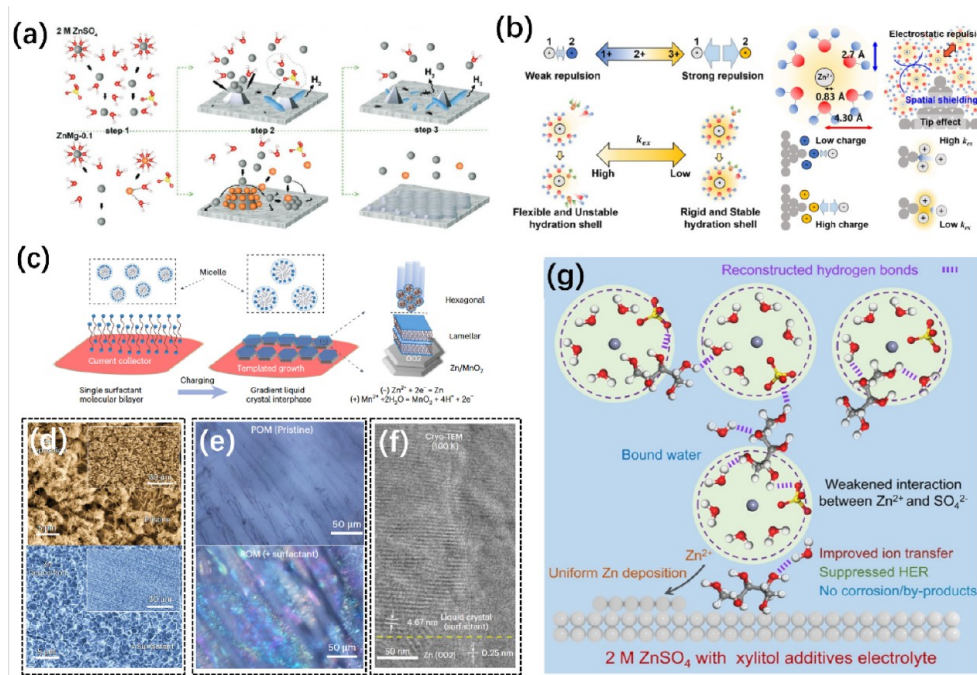


Figure 11. Electrolyte additives and the working mechanisms. (a) Schematics of Zn deposition process in the ZnSO₄ and ZnMg–0.1 electrolyte.¹⁵⁵ Reproduced with permission from ref. 155. Copyright 2021, John Wiley and Sons Inc. (b) Effect of key parameters of redox-inactive cationic additives on tip blocking.¹⁵⁴ Reproduced with permission from ref. 154. Copyright 2022, John Wiley and Sons Inc. (c) Design framework of surfactant additive for Zn/MnO₂ deposition via in situ formed liquid crystal interphase.¹⁶⁸ (d) SEM images of deposited Zn using the pristine electrolyte or surfactant electrolyte.¹⁶⁸ (e) Polarized optical microscope image of Zn surface prepared in the pristine electrolyte or surfactant electrolyte.¹⁶⁸ (f) High resolution cryo-TEM image of the interface between Zn(002) and liquid crystal.¹⁶⁸ Reproduced with permission from ref. 168. Copyright 2024, Springer Nature. (g) Schematic illustration of the Zn²⁺ solvation structures and interfacial chemistry at Zn anodes.⁴⁷ Reproduced with permission from ref. 47. Copyright 2023, John Wiley and Sons Inc.

thereby enabling stable battery cycling performance without compromising sustainability.¹²⁸ Based on a similar principle, the “molecular crowding electrolyte” (MCE) strategy suppresses water activity by increasing the concentration of molecular or polymeric species (as opposed to ionic species) in the electrolyte, disrupting traditional ion solvation structures.^{129,130} In this context, (2-hydroxypropyl)- β -cyclodextrin electrolytes have been invented, which leverage the synergistic effects of an excluded-volume effect and hydrogen-bond networks. These effects substantially lower the activity of water molecules, extend the electrochemical window of the electrolyte, inhibit the dissolution of active materials, and suppress the growth of Zn dendrites (Figure 10e).¹³¹ Furthermore, the hydrogel electrolyte (HGE) can also provide a protective effect on the anode. Featuring polycationic chains and hydrophobic alkyl motifs, the polycationic framework homogenizes interfacial electric fields, confines sulfate anions, and suppresses dendrite growth through preferential Zn (002) crystallization (Figure 10f).¹³² Simultaneously, the hydrophobic domains create a nano-confined water-depleted interface, crucially reducing parasitic water reactivity. The comparison of the four types of electrolytes is summarized in Table 3.

The use of electrolyte additives to facilitate uniform deposition is a prevalent practice in industrial electroplating and is pivotal for augmenting full-cell stability. During the initial cycles of battery cycling, certain electrolyte additives undergo partial decomposition and contribute to the formation of the SEI, which protects the anode, as detailed in Section 3.2. Apart from this, the majority of electrolytes predominantly

enhance the long-term stability of batteries either by adsorbing onto electrode surfaces or by modifying the cation solvation sheath, rather than participating in reactions. In the presence of zinc ions, the potent electric field created by charge accumulation also attracts other positively charged metal cations, leading to their competitive adsorption at protrusions. Alkali metal ions, given their more negative redox potentials, do not experience deposition. Instead, they form an electrostatic shielding layer where Coulombic repulsion inhibits preferential Zn deposition at specific protrusions, promoting a uniform plating morphology.^{154–159} Mg²⁺ exhibits a high binding energy with H₂O, which modifies the Zn²⁺ solvation structure and diminishes H₂O activity (Figure 11a).¹⁵⁵ La³⁺ has the capability to aggregate on the Zn anode surface, decreasing the EDL thickness and reducing the repulsive force between Zn deposits, leading to dense and compact Zn electrodeposition.¹⁵⁶ For a quantitative analysis of the electrostatic shielding effect, the rate constant of the exchange reaction (k_{ex}) is introduced. A smaller k_{ex} value suggests a more rigid solvation shell of ions, demonstrating reduced responsiveness to external disturbances.¹⁵⁴ This rigid solvation shell deters the preferential accumulation of Zn²⁺ at surface protrusions, thus promoting a more homogeneous Zn deposition morphology and enhancing battery cycling stability (Figure 11b).

Organic species, like their counterparts, have the ability to anchor onto Zn anode surfaces via chemisorption and physisorption mechanisms.¹⁶⁰ Chemical adsorption is facilitated through the creation of coordination bonds, utilizing electron pairs from additives and the d orbitals of Zn metal.¹⁶¹

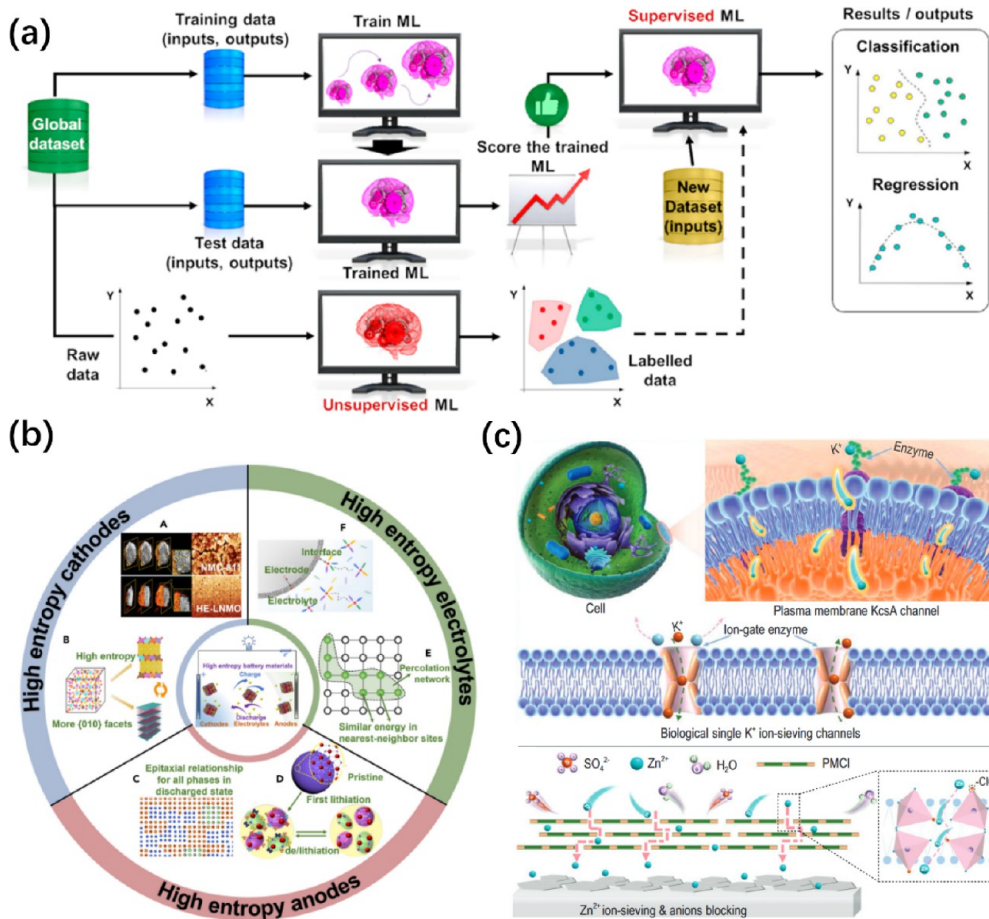


Figure 12. Potential future developments and prospects for AZIBs. (a) Machine learning and artificial intelligence.¹⁷⁵ Reproduced from ref. 175. Copyright 2021, American Chemical Society. (b) High-entropy battery materials design.¹⁷³ Reproduced with permission from ref. 173. Copyright 2023, Elsevier. (c) Bio-inspired structure for electrode material design.¹⁷⁴ Reproduced from ref. 174.

On the other hand, physical adsorption can be accomplished by introducing a small quantity of distinctive organic molecules, which induce uniform ion deposition and regulate the electric double layer structure at the solid–liquid interface.^{8,127,162–167} Among these researches, Li et al. successfully achieved favorable c-axis orientations in hexagonal deposition by incorporating a mere 0.1 mM of surfactant molecules into the electrolyte (Figure 11c–f).¹⁶⁸ This achievement can largely be attributed to the impressive liquid crystal structures formed by the surface-aligned arrangement of amphiphilic molecules, viewable with a polarized optical microscope (Figure 11e). Furthermore, certain electrolyte additives can effectively mitigate side reactions by restructuring hydrogen-bond networks and reorganizing ion solvation shells. Unlike eutectic electrolytes, these additives typically necessitate only minimal concentrations to yield significant functional improvements.^{47,164,169,170} For instance, the use of a 100 mM xylitol additive can weaken electrostatic interaction via oriented reconstruction of hydrogen bonds and suppress the planar diffusion of Zn²⁺ ions through absorption on the surface (Figure 11g).⁴⁷

4. SUMMARY AND PERSPECTIVE

The use of Zn foil as the anode in AZIBs is a straightforward and effective approach to optimizing full-cell energy density. Nevertheless, its intrinsic electrochemical properties and interfacial behaviors are frequently neglected under laboratory

conditions, potentially obscuring key mechanisms of performance degradation. In this review, we conduct a systematic analysis of the inherent characteristics of commonly used commercial Zn foils, including disordered crystallographic orientations, high defect/dislocation densities, and residual stress. These factors are identified as primary contributors to the recurring interfacial instability and electrochemical degradation observed at the anode in AZIBs. Fortunately, simple postprocessing techniques such as rolling and thermal annealing can reconfigure the crystallographic orientation of Zn foils, thereby promoting uniform Zn deposition along the (002) basal plane. This cost-effective strategy offers promising solutions to persistent anode challenges and advances the commercial viability of AZIBs systems. Additionally, we propose complementary strategies to extend the operational lifespan of Zn anodes. These include leveraging heterogeneous substrates to guide uniform Zn deposition, constructing eutectic alloys for enhanced structural stability, engineering high-surface-area 3D architectures to reduce localized current densities, and designing multifunctional gradient-structured anodes via advanced fabrication techniques. These approaches collectively address critical failure modes for long-cycle applications.

Compared with the Li-ion batteries using organic electrolytes, the anode–electrolyte interfaces of aqueous Zn systems suffer more parasitic reactions due to the lack of protective SEI. The in situ formed SEIs usually need fluorinated additives to

stabilize, which may cause environmental pollution problems. Although ASEI layers show higher homogeneity, the complex processes in fabrication raise the production cost. Here, we summarize the critical properties for designing high-performance SEI: (i) high ionic conductivity and low electronic conductivity ensure rapid ion diffusion and deposition while effectively suppressing surface electron exchange-induced side reactions. (ii) a rational design of zincophilic and zincophobic domains is critical to regulate the desolvation of zinc ions and promote their uniform deposition on the anode surface. (iii) excellent chemical stability toward electrolyte decomposition in the operating voltage windows; and (iv) good mechanical properties ensure the anode surface close contact and effectively mitigate the mechanical stresses induced by volume variations during zinc ion insertion and extraction processes.

As a key battery component, the electrolyte not only participates in interfacial reaction pathways, but also in degradation processes that lead to anode failure mechanisms. Conventional aqueous electrolytes based on simple “water + salt” systems have shown fundamental limitations and current research focuses on four major design paradigms: aqueous eutectic electrolytes based on multicomponent solvents, water-in-salt (WIS) strategies based on ultrahigh salt concentrations, molecular crowding electrolytes (MCEs) based on excluded-volume effects, and hydrogel electrolytes based on highly cross-linked polymer matrices. These designs often require the use of organic species, especially for WIS systems where the use of fluorine-containing compounds raises toxicity issues and increases costs, thus making them commercially unviable. On the other hand, electrolyte additives can often significantly increase anode lifetimes at very low concentrations (i.e., 0.1–5 wt %). Organic additives are particularly interesting as they can serve multiple functions by rationally engineering the structure of functional groups (e.g., $-\text{NH}_2/-\text{COOH}/-\text{SH}$), thereby simultaneously modulating both electrochemical thermodynamics and interfacial kinetics.

Despite significant advancements in the theory and technology related to the enhancement of the zinc anode, we posit that there remain several pioneering science and technologies which hold potential for further strengthening the zinc anode. Here, we put forth the following prospects.

4.1. AI-Driven Performance Optimization. Artificial intelligence, as an extremely promising technology, brings boundless possibilities for the future development of science and technology. Machine learning, a branch of it, has begun to be applied in materials research (Figure 12a). For example, the incorporation of specific organic molecules into the electrolyte may result in substantial changes in the anode's enhancement. These organic molecules, owing to their complex carbon chain structures, allow for the fine-tuning of various properties. Utilizing advanced computational techniques combined with artificial intelligence, along with experimental verification, can significantly decrease labor expenses and expedite the development of Zn-ion battery electrolytes and their additives. Indeed, such strategies have already been validated in the existing literature.¹⁷¹ Beyond the direct application of AI to the research and development of novel batteries, some researchers have begun to envision integrating AI into battery systems in an organic manner, proposing the concept of “smart batteries” to anticipate and prepare for future technological advancements.¹⁷²

4.2. High-Entropy Approaches for Optimizing Performance. In prior research, high-entropy materials (HEMs) have exhibited remarkable characteristics such as structural stabilization driven by configurational entropy, improved redox reversibility, optimized ion transport kinetics, and synergistic “cocktail effects” resulting from multi-element coordination. These principles can be leveraged to apply similar entropy engineering tactics for the logical design of the anode, cathode and advanced electrolytes (Figure 12b).¹⁷³ For example, integrating multi-component synergistic interactions at the electrode–electrolyte interfaces could maintain the mechanical integrity of SEI under continuous stripping/plating. Additionally, the multicomponent complexity of high-entropy materials often imply an astronomically vast combination space, such that integrating computational materials science with AI techniques may significantly accelerate their development.

4.3. Bio-Inspired Strategies to Boost Zn Anode Performance. The operation of zinc-ion batteries frequently involve mass diffusion and ion transport processes. Taking inspiration from the efficient and selective transport mechanisms in biological systems, a new research direction is emerging (Figure 12c).¹⁷⁴ This approach abstracts and concretely applies these mechanisms to develop innovative strategies for constructing SEIs with dual characteristics of rapid ion conduction and enhanced selectivity. Moreover, this paradigm may guide the design of anode materials with tailored architectures or specialized functionalities, facilitating the development of long-term and stable zinc-ion storage systems. This biomimetic design philosophy offers a promising avenue for enhancing next-generation energy storage technologies.

■ AUTHOR INFORMATION

Corresponding Authors

Wenshu Chen – School of Materials Science and Engineering, Southeast University, Nanjing 211189, PR China;
Email: 101013800@seu.edu.cn

Pan Feng – School of Materials Science and Engineering, Southeast University, Nanjing 211189, PR China; State Key Laboratory of Engineering Materials for Major Infrastructure and Jiangsu Key Laboratory of Construction Materials, Southeast University, Nanjing 211189, PR China;
 orcid.org/0000-0002-2692-5971; Email: pan.feng@seu.edu.cn

Linfeng Hu – School of Materials Science and Engineering, Southeast University, Nanjing 211189, PR China; Z Energy Storage Center, Southeast University, Nanjing 211189, PR China;  orcid.org/0000-0002-0640-508X;
Email: linfenghu@fudan.edu.cn

Authors

Shuo Liu – School of Materials Science and Engineering, Southeast University, Nanjing 211189, PR China

Xiaoyue Li – School of Materials Science and Engineering, Southeast University, Nanjing 211189, PR China

Mengyao Qin – School of Materials Science and Engineering, Southeast University, Nanjing 211189, PR China

Shuyang Bian – School of Materials Science and Engineering, Southeast University, Nanjing 211189, PR China

Fei Ye – Nanjing Polytechnic Institute, Nanjing 210044, PR China

Yuping Wu – School of Energy and Environment, Southeast University, Nanjing 211189, PR China; Z Energy Storage

Center, Southeast University, Nanjing 211189, PR China;
orcid.org/0000-0002-0833-1205

Complete contact information is available at:
<https://pubs.acs.org/10.1021/acsaem.Sc00640>

Notes

The authors declare no competing financial interest.

ACKNOWLEDGMENTS

This work was financially supported by the National Key Research and Development Program of China (Grant Nos. 2024YFB3715000 and 2021YFB2400400), National Natural Science Foundation of China (Grant Nos. 52371214, 52171203, and 52302224), the Natural Science Foundation of Jiangsu Province (Grant No. BK20221179).

REFERENCES

- (1) Ji, X. A Paradigm of Storage Batteries. *Energy Environ. Sci.* **2019**, *12* (11), 3203–3224.
- (2) Pomerantseva, E.; Bonaccorso, F.; Feng, X.; Cui, Y.; Gogotsi, Y. Energy Storage: The Future Enabled by Nanomaterials. *Science* **2019**, *366* (6468), No. eaan8285.
- (3) Zhang, N.; Chen, X.; Yu, M.; Niu, Z.; Cheng, F.; Chen, J. Materials Chemistry for Rechargeable Zinc–Ion Batteries. *Chem. Soc. Rev.* **2020**, *49* (13), 4203–4219.
- (4) Zhao, C.; Zhang, Y.; Gao, J.; Guo, Z.; Chen, A.; Liu, N.; Lu, X.; Zhang, X.; Zhang, N. Zincophilic Design and the Electrode/Electrolyte Interface for Aqueous Zinc–Ion Batteries: A Review. *Batteries Supercaps* **2023**, *6* (5), No. e202200478.
- (5) Yang, J.; Yin, B.; Sun, Y.; Pan, H.; Sun, W.; Jia, B.; Zhang, S.; Ma, T. Zinc Anode for Mild Aqueous Zinc–Ion Batteries: Challenges, Strategies, and Perspectives. *Nano–Micro Lett.* **2022**, *14* (1), 42.
- (6) Chen, Z.; Zhao, J.; He, Q.; Li, M.; Feng, S.; Wang, Y.; Yuan, D.; Chen, J.; Alshareef, H. N.; Ma, Y. Texture Control of Commercial Zn Foils Prolongs Their Reversibility as Aqueous Battery Anodes. *ACS Energy Lett.* **2022**, *7* (10), 3564–3571.
- (7) Chen, Z.; Wu, Q.; Han, X.; Wang, C.; Chen, J.; Hu, T.; He, Q.; Zhu, X.; Yuan, D.; Chen, J.; Zhang, Y.; Yang, L.; Ma, Y.; Zhao, J. Converting Commercial Zn Foils into Single (002)-Textured Zn with Millimeter-Sized Grains for Highly Reversible Aqueous Zinc Batteries. *Angew. Chem. Int. Ed.* **2024**, *63* (17), No. e202401507.
- (8) Zhao, Q.; Stalin, S.; Archer, L. A. Stabilizing Metal Battery Anodes through the Design of Solid Electrolyte Interphases. *Joule* **2021**, *5* (5), 1119–1142.
- (9) Zhang, R.; Cheng, X.; Zhao, C.; Peng, H.; Shi, J.; Huang, J.; Wang, J.; Wei, F.; Zhang, Q. Conductive Nanostructured Scaffolds Render Low Local Current Density to Inhibit Lithium Dendrite Growth. *Adv. Mater.* **2016**, *28* (11), 2155–2162.
- (10) Wei, T.; Zhang, H.; Ren, Y.; Mo, L.; He, Y.; Tan, P.; Huang, Y.; Li, Z.; Zhu, D.; Hu, L. Building Near-Unity Stacked (002) Texture for High-Stable Zinc Anode. *Adv. Funct. Mater.* **2024**, *34* (14), 2312506.
- (11) Ren, B.; Zhang, X.; Wei, H.; Jiang, J.; Chen, G.; Li, H.; Liu, Z. Suppressing Zinc Metal Corrosion by an Effective and Durable Corrosion Inhibitor for Stable Aqueous Zinc Batteries. *Adv. Funct. Mater.* **2024**, *35* (17), 2418594.
- (12) Zhang, H.; Zhu, G.; Lu, J.; Hou, Y.; Bao, Y.; Liu, P.; Zhang, Y. 3D Printing-Induced Phase Transition in Ferroelectric Porous Polymer Coatings for Stable Zinc Anodes. *Small* **2025**, *21* (4), 2408848.
- (13) Liu, Z.; Guo, Z.; Fan, L.; Zhao, C.; Chen, A.; Wang, M.; Li, M.; Lu, X.; Zhang, J.; Zhang, Y.; Zhang, N. Construct Robust Epitaxial Growth of (101) Textured Zinc Metal Anode for Long Life and High Capacity in Mild Aqueous Zinc–Ion Batteries. *Adv. Mater.* **2024**, *36* (5), 2305988.
- (14) Guo, X.; He, G. Opportunities and Challenges of Zinc Anodes in Rechargeable Aqueous Batteries. *J. Mater. Chem. A* **2023**, *11* (23), 11987–12001.
- (15) Zhang, X.; Li, J.; Liu, Y.; Lu, B.; Liang, S.; Zhou, J. Single [0001]–Oriented Zinc Metal Anode Enables Sustainable Zinc Batteries. *Nat. Commun.* **2024**, *15* (1), 2735.
- (16) Zhou, M.; Guo, S.; Li, J.; Luo, X.; Liu, Z.; Zhang, T.; Cao, X.; Long, M.; Lu, B.; Pan, A.; Fang, G.; Zhou, J.; Liang, S. Surface-Preferred Crystal Plane for a Stable and Reversible Zinc Anode. *Adv. Mater.* **2021**, *33* (21), 2100187.
- (17) Li, Y.; Peng, C.; Gao, X.; Liu, H.; Wang, W. Stress Relief and Crystal Face Transition Process Contribute to the Stability of Zinc Anodes. *J. Energy Chem.* **2024**, *99*, 593–603.
- (18) Zheng, J.; Deng, Y.; Yin, J.; Tang, T.; Garcia-Mendez, R.; Zhao, Q.; Archer, L. A. Textured Electrodes: Manipulating Built-In Crystallographic Heterogeneity of Metal Electrodes via Severe Plastic Deformation. *Adv. Mater.* **2022**, *34* (1), 2106867.
- (19) Ren, L.; Hu, Z.; Peng, C.; Zhang, L.; Wang, N.; Wang, F.; Xia, Y.; Zhang, S.; Hu, E.; Luo, J. Suppressing Metal Corrosion through Identification of Optimal Crystallographic Plane for Zn Batteries. *Proc. Natl. Acad. Sci. U. S. A.* **2024**, *121* (5), No. e2309981121.
- (20) Chen, J.; Xu, Y.; Wang, Y.; Lv, Z.; Zhang, S.; Dong, W.; Hou, J.; Fang, Y.; Bi, H.; Huang, F. Molecular Key Tuned Steric–Hindrance Effect toward Zn (100) Facet Texture Anode. *Energy Storage Mater.* **2024**, *72*, 103765.
- (21) Zhu, Q.; Sun, G.; Qiao, S.; Wang, D.; Cui, Z.; Zhang, W.; Liu, J. Selective Shielding of the (002) Plane Enabling Vertically Oriented Zinc Plating for Dendrite-Free Zinc Anode. *Adv. Mater.* **2024**, *36* (11), 2308577.
- (22) Ren, Q.; Tang, X.; Guo, Y.; Liao, X.; Zhang, C.; Zhu, Z.; Wang, P.; Wang, W.; Li, Y.; Song, W.; Wang, S.; He, K.; Wang, Z.; Yuan, Y. Achieving the Dendrite-Free Zn Anode by Inducing the (101)-Preferred Electrodeposition of Zn Crystals. *Adv. Energy Mater.* **2025**, *15* (9), 2403961.
- (23) Kasemchainan, J.; Zekoll, S.; Spencer Jolly, D.; Ning, Z.; Hartley, G. O.; Marrow, J.; Bruce, P. G. Critical Stripping Current Leads to Dendrite Formation on Plating in Lithium Anode Solid Electrolyte Cells. *Nat. Mater.* **2019**, *18* (10), 1105–1111.
- (24) Xie, C.; Liu, S.; Yang, Z.; Ji, H.; Zhou, S.; Wu, H.; Hu, C.; Tang, Y.; Ji, X.; Zhang, Q.; Wang, H. Discovering the Intrinsic Causes of Dendrite Formation in Zinc Metal Anodes: Lattice Defects and Residual Stress. *Angew. Chem. Int. Ed.* **2023**, *62* (16), No. e202218612.
- (25) Huang, S.; Wu, W.; Su, Y.; Qiao, L.; Yan, Y. Insight into the Corrosion Behaviour and Degradation Mechanism of Pure Zinc in Simulated Body Fluid. *Corros. Sci.* **2021**, *178*, 109071.
- (26) Jia, X.; Liu, C.; Neale, Z. G.; Yang, J.; Cao, G. Active Materials for Aqueous Zinc Ion Batteries: Synthesis, Crystal Structure, Morphology, and Electrochemistry. *Chem. Rev.* **2020**, *120* (15), 7795–7866.
- (27) Zhao, Y.; Guo, S.; Chen, M.; Lu, B.; Zhang, X.; Liang, S.; Zhou, J. Tailoring Grain Boundary Stability of Zinc–Titanium Alloy for Long-Lasting Aqueous Zinc Batteries. *Nat. Commun.* **2023**, *14* (1), 7080.
- (28) Zheng, Z.; Zhong, X.; Zhang, Q.; Zhang, M.; Dai, L.; Xiao, X.; Xu, J.; Jiao, M.; Wang, B.; Li, H.; Jia, Y.; Mao, R.; Zhou, G. An Extended Substrate Screening Strategy Enabling a Low Lattice Mismatch for Highly Reversible Zinc Anodes. *Nat. Commun.* **2024**, *15* (1), 753.
- (29) Wang, D.; Zhang, W.; Zheng, W.; Cui, X.; Rojo, T.; Zhang, Q. Towards High-Safe Lithium Metal Anodes: Suppressing Lithium Dendrites via Tuning Surface Energy. *Adv. Sci.* **2017**, *4* (1), 1600168.
- (30) Cao, J.; Shi, Y.; Gao, A.; Du, G.; Dilxat, M.; Zhang, Y.; Cai, M.; Qian, G.; Lu, X.; Xie, F.; Sun, Y.; Lu, X. Hierarchical Li Electrochemistry Using Alloy-Type Anode for High-Energy-Density Li Metal Batteries. *Nat. Commun.* **2024**, *15* (1), 1354.
- (31) Yi, Z.; Liu, J.; Tan, S.; Sang, Z.; Mao, J.; Yin, L.; Liu, X.; Wang, L.; Hou, F.; Dou, S. X.; Cheng, H.; Liang, J. An Ultrahigh Rate and Stable Zinc Anode by Facet-Matching-Induced Dendrite Regulation. *Adv. Mater.* **2022**, *34* (37), 2203835.
- (32) Ji, J.; Zhu, Z.; Du, H.; Qi, X.; Yao, J.; Wan, H.; Wang, H.; Qie, L.; Huang, Y. Zinc-Contained Alloy as a Robustly Adhered Interfacial

- Lattice Locking Layer for Planar and Stable Zinc Electrodeposition. *Adv. Mater.* **2023**, *35* (20), 2211961.
- (33) Guo, R.; Liu, X.; Ni, K.; Xia, F.; Zhang, H.; Liu, Y.; Dai, X.; Shi, L.; Wang, X.; Han, C.; Mai, L.; Niu, C. Non-Destructive Stripping Electrochemistry Enables Long-Life Zinc Metal Batteries. *Energy Environ. Sci.* **2025**, *18*, 2353–2364.
- (34) Li, T. C.; Lim, Y. V.; Xie, X.; Li, X. L.; Li, G.; Fang, D.; Li, Y.; Ang, Y. S.; Ang, L. K.; Yang, H. Y. ZnSe Modified Zinc Metal Anodes: Toward Enhanced Zincophilicity and Ionic Diffusion. *Small* **2021**, *17* (35), 2101728.
- (35) Zheng, J.; Zhao, Q.; Tang, T.; Yin, J.; Quilty, C. D.; Renderos, G. D.; Liu, X.; Deng, Y.; Wang, L.; Bock, D. C.; Jaye, C.; Zhang, D.; Takeuchi, E. S.; Takeuchi, K. J.; Marschilok, A. C.; Archer, L. A. Reversible Epitaxial Electrodeposition of Metals in Battery Anodes. *Science* **2019**, *366* (6465), 645–648.
- (36) Du, Y.; Feng, Y.; Li, R.; Peng, Z.; Yao, X.; Duan, S.; Liu, S.; Jun, S. C.; Zhu, J.; Dai, L.; Yang, Q.; Wang, L.; He, Z. Zinc-Bismuth Binary Alloy Enabling High-Performance Aqueous Zinc Ion Batteries. *Small* **2024**, *20* (17), 2307848.
- (37) Fan, W.; Li, P.; Shi, J.; Chen, J.; Tian, W.; Wang, H.; Wu, J.; Yu, G. Atomic Zincophilic Sites Regulating Microspace Electric Fields for Dendrite-Free Zinc Anode. *Adv. Mater.* **2024**, *36* (1), 2307219.
- (38) Lu, H.; Jin, Q.; Jiang, X.; Dang, Z.; Zhang, D.; Jin, Y. Vertical Crystal Plane Matching between AgZn₃ (002) and Zn (002) Achieving a Dendrite-Free Zinc Anode. *Small* **2022**, *18* (16), 2200131.
- (39) Liu, H.; Xu, Z.; Cao, B.; Xin, Z.; Lai, H.; Gao, S.; Xu, B.; Yang, J.; Xiao, T.; Zhang, B.; Fan, H. J. Marangoni-Driven Self-Assembly MXene As Functional Membrane Enables Dendrite-Free and Flexible Zinc-Iodine Pouch Cells. *Adv. Energy Mater.* **2024**, *14* (26), 2400318.
- (40) Fu, J.; Cano, Z. P.; Park, M. G.; Yu, A.; Fowler, M.; Chen, Z. Electrically Rechargeable Zinc–Air Batteries: Progress, Challenges, and Perspectives. *Adv. Mater.* **2017**, *29* (7), 1604685.
- (41) Zhou, J.; Wu, F.; Mei, Y.; Hao, Y.; Li, L.; Xie, M.; Chen, R. Establishing Thermal Infusion Method for Stable Zinc Metal Anodes in Aqueous Zinc-Ion Batteries. *Adv. Mater.* **2022**, *34* (21), 2200782.
- (42) Zeng, L.; He, J.; Yang, C.; Luo, D.; Yu, H.; He, H.; Zhang, C. Direct 3D Printing of Stress-Released Zn Powder Anodes toward Flexible Dendrite-Free Zn Batteries. *Energy Storage Mater.* **2023**, *54*, 469–477.
- (43) Zhang, G.; Zhang, X.; Liu, H.; Li, J.; Chen, Y.; Duan, H. 3D-Printed Multi-Channel Metal Lattices Enabling Localized Electric-Field Redistribution for Dendrite-Free Aqueous Zn Ion Batteries. *Adv. Energy Mater.* **2021**, *11* (19), 2003927.
- (44) Zhu, M.; Wang, H.; Wang, H.; Li, C.; Chen, D.; Wang, K.; Bai, Z.; Chen, S.; Zhang, Y.; Tang, Y. A Fluorinated Solid-state-electrolyte Interface Layer Guiding Fast Zinc-ion Oriented Deposition in Aqueous Zinc-ion Batteries. *Angew. Chem. Int. Ed.* **2024**, *63* (4), No. e202316904.
- (45) Zhao, M.; Lv, Y.; Qi, J.; Zhang, Y.; Du, Y.; Yang, Q.; Xu, Y.; Qiu, J.; Lu, J.; Chen, S. Crystallographic Reorientation Induced by Gradient Solid-Electrolyte Interphase for Highly Stable Zinc Anode. *Adv. Mater.* **2024**, *36* (52), 2412667.
- (46) Lee, J.-H.; Kim, R.; Kim, S.; Heo, J.; Kwon, H.; Yang, J. H.; Kim, H.-T. Dendrite-Free Zn Electrodeposition Triggered by Interatomic Orbital Hybridization of Zn and Single Vacancy Carbon Defects for Aqueous Zn-Based Flow Batteries. *Energy Environ. Sci.* **2020**, *13* (9), 2839–2848.
- (47) Wang, H.; Ye, W.; Yin, B.; Wang, K.; Riaz, M. S.; Xie, B.; Zhong, Y.; Hu, Y. Modulating Cation Migration and Deposition with Xylitol Additive and Oriented Reconstruction of Hydrogen Bonds for Stable Zinc Anodes. *Angew. Chem. Int. Ed.* **2023**, *62* (10), No. e202218872.
- (48) Chen, K.; Chen, Y.; Xu, Y.; Xu, M.; Li, Y.; Yang, S.; Wu, Q.; Xu, Q.; Xie, H.; Huang, J. Regulating Interfacial Chemistry with Biobased Multifunctional Cellulose Levulinate Ester for Highly Reversible Zinc Ion Batteries. *Energy Storage Mater.* **2024**, *71*, 103597.
- (49) Wang, S.-B.; Ran, Q.; Yao, R.-Q.; Shi, H.; Wen, Z.; Zhao, M.; Lang, X.-Y.; Jiang, Q. Lamella–Nanostructured Eutectic Zinc–Aluminum Alloys as Reversible and Dendrite-Free Anodes for Aqueous Rechargeable Batteries. *Nat. Commun.* **2020**, *11* (1), 1634.
- (50) Zheng, J.; Huang, Z.; Zeng, Y.; Liu, W.; Wei, B.; Qi, Z.; Wang, Z.; Xia, C.; Liang, H. Electrostatic Shielding Regulation of Magnetron Sputtered Al-Based Alloy Protective Coatings Enables Highly Reversible Zinc Anodes. *Nano Lett.* **2022**, *22* (3), 1017–1023.
- (51) Li, H.; Zhao, R.; Zhou, W.; Wang, L.; Li, W.; Zhao, D.; Chao, D. Trade-off between Zincophilicity and Zincophobicity: Toward Stable Zn-Based Aqueous Batteries. *JACS Au.* **2023**, *3* (8), 2107–2116.
- (52) Zeng, W.; Wei, P.; Chen, J.; Wang, G.; Yan, Y.; Yu, H.; Yang, C.; Zhang, G.; Jiang, H. Ultra-Stable Zinc Metal Anodes Enabled by Uniform Zn Deposition on A Preferential Crystal Plane. *Adv. Energy Mater.* **2023**, *13* (41), 2302205.
- (53) Pan, Z.; Cao, Q.; Gong, W.; Yang, J.; Gao, Y.; Gao, Y.; Pu, J.; Sun, J.; Loh, X. J.; Liu, Z.; Guan, C.; Wang, J. Zincophilic 3D ZnOHF Nanowire Arrays with Ordered and Continuous Zn²⁺ Ion Modulation Layer Enable Long-Term Stable Zn Metal Anodes. *Energy Storage Mater.* **2022**, *50*, 435–443.
- (54) Cao, Q.; Pan, Z.; Gao, Y.; Pu, J.; Fu, G.; Cheng, G.; Guan, C. Stable Imprinted Zincophilic Zn Anodes with High Capacity. *Adv. Funct. Mater.* **2022**, *32* (41), 2205771.
- (55) Cao, Q.; Gao, Y.; Pu, J.; Zhao, X.; Wang, Y.; Chen, J.; Guan, C. Gradient Design of Imprinted Anode for Stable Zn–Ion Batteries. *Nat. Commun.* **2023**, *14* (1), 641.
- (56) Gao, Y.; Cao, Q.; Pu, J.; Zhao, X.; Fu, G.; Chen, J.; Wang, Y.; Guan, C. Stable Zn Anodes with Triple Gradients. *Adv. Mater.* **2023**, *35* (6), 2207573.
- (57) Mu, Y.; Li, Z.; Wu, B.; Huang, H.; Wu, F.; Chu, Y.; Zou, L.; Yang, M.; He, J.; Ye, L.; Han, M.; Zhao, T.; Zeng, L. 3D Hierarchical Graphene Matrices Enable Stable Zn Anodes for Aqueous Zn Batteries. *Nat. Commun.* **2023**, *14* (1), 4205.
- (58) Zhang, Z.; Xia, S.; Dong, A.; Li, X.; Wang, F.; Yang, J.; Ruan, J.; Li, Q.; Sun, D.; Fang, F.; Liu, Y.; Wang, F. Mechanical Grinding Formation of Highly Reversible (002)-Textured Zinc Metal Anodes. *Adv. Energy Mater.* **2024**, *15* (8), 2403598.
- (59) Long, X.; Liu, Y.; Wang, D.; Nie, Y.; Lai, X.; Luo, D.; Wang, X. Electric Field Distribution Regulation of a Zinc Anode toward Long Cycle Life Zinc Metal Batteries. *J. Mater. Chem. A* **2024**, *12* (22), 13181–13190.
- (60) Yang, Z.; Hu, C.; Zhang, Q.; Wu, T.; Xie, C.; Wang, H.; Tang, Y.; Ji, X.; Wang, H. Bulk-Phase Reconstruction Enables Robust Zinc Metal Anodes for Aqueous Zinc-Ion Batteries. *Angew. Chem. Int. Ed.* **2023**, *62* (35), No. e202308017.
- (61) Yan, M.; Zhao, X.; Chen, D.; Li, W.; Liu, L.; Sun, Y.; Jiao, S.; Pan, H. Crystal Step-Induced Uniform and Rapid Deposition on Zinc Anodes. *Adv. Energy Mater.* **2025**, *15* (6), 2403860.
- (62) Zhou, X.; Wen, B.; Cai, Y.; Chen, X.; Li, L.; Zhao, Q.; Chou, S.; Li, F. Interfacial Engineering for Oriented Crystal Growth toward Dendrite-Free Zn Anode for Aqueous Zinc Metal Battery. *Angew. Chem. Int. Ed.* **2024**, *63* (21), No. e202402342.
- (63) Zhang, S.; Li, J.; Jin, B.; Shao, M. Oriented Zinc Metal Anode Based on Directional Recognition and Assembly. *Small* **2023**, *19* (38), 2301874.
- (64) Zhang, B.; Fan, H. J. Overlooked Calendar Issues of Aqueous Zinc Metal Batteries. *Joule* **2025**, *9* (1), 101802.
- (65) Tian, S.; Hwang, T.; Zhang, Z.; Wu, S.; Mashhadian, A.; Zhang, R.; Milazzo, T.; Luo, T.; Jian, R.; Li, T.; Cho, K.; Xiong, G. Transforming Detrimental Crystalline Zinc Hydroxide Sulfate to Homogeneous Fluorinated Amorphous Solid–Electrolyte Interphase on Zinc Anode. *ACS Nano* **2025**, *19* (3), 3135–3146.
- (66) Hao, J.; Li, B.; Li, X.; Zeng, X.; Zhang, S.; Yang, F.; Liu, S.; Li, D.; Wu, C.; Guo, Z. An In-Depth Study of Zn Metal Surface Chemistry for Advanced Aqueous Zn-Ion Batteries. *Adv. Mater.* **2020**, *32* (34), 2003021.
- (67) Yuan, W.; Ma, G.; Nie, X.; Wang, Y.; Di, S.; Wang, L.; Wang, J.; Shen, S.; Zhang, N. In-Situ Construction of a Hydroxide-Based

- Solid Electrolyte Interphase for Robust Zinc Anodes. *Chem. Eng. J.* **2022**, *431*, 134076.
- (68) Zhou, A.; Wang, H.; Hu, X.; Hu, Z.; Zhao, Y.; Zhang, B.; Huang, Y.; Cui, Y.; Cui, Y.; Li, L.; Wu, F.; Chen, R. Synergy of In Situ Heterogeneous Interphases with Hydrogen Bond Reconstruction Enabling Highly Reversible Zn Anode at -40°C . *Adv. Funct. Mater.* **2025**, *35* (4), 2413807.
- (69) Cui, M.; Yu, L.; Hu, J.; He, S.; Zhi, C.; Huang, Y. Tailored Polymer-Inorganic Bilayer SEI with Proton Holder Feature for Aqueous Zn Metal Batteries. *Angew. Chem. Int. Ed.* **2025**, *64* (14), No. e202423531.
- (70) Chen, X.; Liu, C.; Bai, X.; Zhang, J.; Chang, X.; Hou, L.; Huang, H.; Wei, Y.; Wu, B.; Liu, W.; Wang, Q. A Thin and Homogeneous Solid Electrolyte Interface Enriched with ZnF_2 and ZnS for Highly Reversible Zinc Batteries. *Energy Storage Mater.* **2025**, *75*, 103984.
- (71) Ma, L.; Li, Q.; Ying, Y.; Ma, F.; Chen, S.; Li, Y.; Huang, H.; Zhi, C. Toward Practical High-Areal-Capacity Aqueous Zinc-Metal Batteries: Quantifying Hydrogen Evolution and a Solid-Ion Conductor for Stable Zinc Anodes. *Adv. Mater.* **2021**, *33* (12), 2007406.
- (72) Wang, D.; Peng, H.; Zhang, S.; Liu, H.; Wang, N.; Yang, J. Localized Anion-Cation Aggregated Aqueous Electrolytes with Accelerated Kinetics for Low-Temperature Zinc Metal Batteries. *Angew. Chem. Int. Ed.* **2023**, *62* (50), No. e202315834.
- (73) Liu, S.; Vongsivut, J.; Wang, Y.; Zhang, R.; Yang, F.; Zhang, S.; Davey, K.; Mao, J.; Guo, Z. Monolithic Phosphate Interphase for Highly Reversible and Stable Zn Metal Anode. *Angew. Chem., Int. Ed.* **2023**, *135* (4), No. e202215600.
- (74) Zhang, W.; He, G. Solid-Electrolyte Interphase Chemistries Towards High-Performance Aqueous Zinc Metal Batteries. *Angew. Chem., Int. Ed.* **2023**, *135* (13), No. e202218466.
- (75) Wang, Y.; Wang, T.; Cui, P.; Mao, G.; Ye, K.; Hu, F.; Chen, M.; Cao, D.; Zhu, K. Phosphated Electrolyte Enabling Dual Robust Electrode–Electrolyte Interfacial Reconstruction Toward Capable Zn Metal Batteries. *Adv. Funct. Mater.* **2025**, *35*, 2421363.
- (76) Lyu, H.; Zhao, S.; Liao, C.; Li, G.; Zhi, J.; Huang, F. Electric Double Layer Oriented Eutectic Additive Design toward Stable Zn Anodes with a High Depth of Discharge. *Adv. Mater.* **2024**, *36* (29), 2400976.
- (77) Wang, W.; Chen, S.; Liao, X.; Huang, R.; Wang, F.; Chen, J.; Wang, Y.; Wang, F.; Wang, H. Regulating Interfacial Reaction through Electrolyte Chemistry Enables Gradient Interphase for Low-Temperature Zinc Metal Batteries. *Nat. Commun.* **2023**, *14* (1), 5443.
- (78) Qin, S.; Zhang, J.; Xu, M.; Xu, P.; Zou, J.; Li, J.; Luo, D.; Zhang, Y.; Dou, H.; Chen, Z. Formulating Self-Repairing Solid Electrolyte Interface via Dynamic Electric Double Layer for Practical Zinc Ion Batteries. *Angew. Chem. Int. Ed.* **2024**, *63* (42), No. e202410422.
- (79) Li, Y.; Yu, Z.; Huang, J.; Wang, Y.; Xia, Y. Constructing Solid Electrolyte Interphase for Aqueous Zinc Batteries. *Angew. Chem., Int. Ed.* **2023**, *135* (47), No. e202309957.
- (80) Cao, L.; Li, D.; Pollard, T.; Deng, T.; Zhang, B.; Yang, C.; Chen, L.; Vatamanu, J.; Hu, E.; Hourwitz, M. J.; Ma, L.; Ding, M.; Li, Q.; Hou, S.; Gaskell, K.; Fourkas, J. T.; Yang, X. –; Xu, K.; Borodin, O.; Wang, C. Fluorinated Interphase Enables Reversible Aqueous Zinc Battery Chemistries. *Nat. Nanotechnol.* **2021**, *16* (8), 902–910.
- (81) Sha, D.; Lu, C.; Hu, R.; Bao, Z.; Pan, L.; Sun, Z. Exploiting Bifunctional ZnTe for Zn Anode Protection and Conversion-Type Cathode toward Compatible Aqueous Zn–Ion Batteries. *Energy Storage Mater.* **2024**, *66*, 103228.
- (82) Cao, P.; Zhou, X.; Wei, A.; Meng, Q.; Ye, H.; Liu, W.; Tang, J.; Yang, J. Fast-Charging and Ultrahigh-Capacity Zinc Metal Anode for High-Performance Aqueous Zinc-Ion Batteries. *Adv. Funct. Mater.* **2021**, *31* (20), 2100398.
- (83) Zhang, H.; You, Y.; Sha, D.; Shui, T.; Moloto, N.; Liu, J.; Kure-Chu, S.; Hihara, T.; Zhang, W.; Sun, Z. Planar Deposition via In Situ Conversion Engineering for Dendrite-Free Zinc Batteries. *Adv. Mater.* **2024**, *36* (44), 2409763.
- (84) Zhou, W.; Chen, Z.; Zhao, S.; Chen, S. Superhydrophobic and Highly Flexible Artificial Solid Electrolyte Interphase Inspired by Lotus Effect Toward Highly Stable Zn Anode. *Adv. Funct. Mater.* **2024**, *34* (49), 2409520.
- (85) Zhang, X.; Li, J.; Liu, D.; Liu, M.; Zhou, T.; Qi, K.; Shi, L.; Zhu, Y.; Qian, Y. Ultra–Long–Life and Highly Reversible Zn Metal Anodes Enabled by a Desolvation and Deionization Interface Layer. *Energy Environ. Sci.* **2021**, *14* (5), 3120–3129.
- (86) Zhang, N.; Huang, S.; Yuan, Z.; Zhu, J.; Zhao, Z.; Niu, Z. Direct Self-Assembly of MXene on Zn Anodes for Dendrite-Free Aqueous Zinc-Ion Batteries. *Angew. Chem. Int. Ed.* **2021**, *60* (6), 2861–2865.
- (87) Zhang, R.; Feng, Y.; Ni, Y.; Zhong, B.; Peng, M.; Sun, T.; Chen, S.; Wang, H.; Tao, Z.; Zhang, K. Bifunctional Interphase with Target-Distributed Desolvation Sites and Directionally Depositional Ion Flux for Sustainable Zinc Anode. *Angew. Chem. Int. Ed.* **2023**, *62* (25), No. e202304503.
- (88) Wang, Y.; Liu, Y.; Wang, H.; Dou, S.; Gan, W.; Ci, L.; Huang, Y.; Yuan, Q. MOF-Based Ionic Sieve Interphase for Regulated Zn^{2+} Flux toward Dendrite-Free Aqueous Zinc-Ion Batteries. *J. Mater. Chem. A* **2022**, *10* (8), 4366–4375.
- (89) Yang, H.; Chang, Z.; Qiao, Y.; Deng, H.; Mu, X.; He, P.; Zhou, H. Constructing a Super-Saturated Electrolyte Front Surface for Stable Rechargeable Aqueous Zinc Batteries. *Angew. Chem. Int. Ed.* **2020**, *59* (24), 9377–9381.
- (90) Guo, X.; Lu, J.; Wang, M.; Chen, A.; Hong, H.; Li, Q.; Zhu, J.; Wang, Y.; Yang, S.; Huang, Z.; Wang, Y.; Pei, Z.; Zhi, C. Solid–Electrolyte Interphase Governs Zinc Ion Transfer Kinetics in High-Rate and Stable Zinc Metal Batteries. *Chem* **2024**, *10* (12), 3607–3621.
- (91) Zhang, Q.; Luan, J.; Huang, X.; Wang, Q.; Sun, D.; Tang, Y.; Ji, X.; Wang, H. Revealing the Role of Crystal Orientation of Protective Layers for Stable Zinc Anode. *Nat. Commun.* **2020**, *11* (1), 3961.
- (92) Shao, Z.; Lin, L.; Zhuang, W.; Liu, S.; Yang, P.; Zhu, K.; Li, C.; Guo, G.; Wang, W.; Zhang, Q.; Yao, Y. Itu Self-Reconfiguration Induced Multifunctional Triple-Gradient Artificial Interfacial Layer toward Long-Life Zn-Metal Anodes. *Adv. Mater.* **2024**, *36* (32), 2406093.
- (93) Cao, L.; Li, D.; Soto, F. A.; Ponce, V.; Zhang, B.; Ma, L.; Deng, T.; Seminario, J. M.; Hu, E.; Yang, X.; Balbuena, P. B.; Wang, C. Highly Reversible Aqueous Zinc Batteries Enabled by Zincophilic–Zincophobic Interfacial Layers and Interrupted Hydrogen-Bond Electrolytes. *Angew. Chem. Int. Ed.* **2021**, *60* (34), 18845–18851.
- (94) Zhang, X.; Su, L.; Lu, F.; Tian, Y.; Xie, F.; Liang, L.; Zheng, L.; Gao, X. Tailoring the Hydrophobicity and Zincophilicity of Poly(Ionic Liquid) Solid–Electrolyte Interphases for Ultra–Stable Aqueous Zinc Batteries. *Green Chem.* **2023**, *25* (21), 8759–8769.
- (95) Yan, H.; Li, S.; Nan, Y.; Yang, S.; Li, B. Ultrafast Zinc–Ion–Conductor Interface toward High-Rate and Stable Zinc Metal Batteries. *Adv. Energy Mater.* **2021**, *11* (18), 2100186.
- (96) Deng, C.; Xie, X.; Han, J.; Tang, Y.; Gao, J.; Liu, C.; Shi, X.; Zhou, J.; Liang, S. A Sieve-Functional and Uniform-Porous Kaolin Layer toward Stable Zinc Metal Anode. *Adv. Funct. Mater.* **2020**, *30* (21), 2000599.
- (97) Kang, L.; Cui, M.; Jiang, F.; Gao, Y.; Luo, H.; Liu, J.; Liang, W.; Zhi, C. Nanoporous CaCO_3 Coatings Enabled Uniform Zn Stripping/Plating for Long-Life Zinc Rechargeable Aqueous Batteries. *Adv. Energy Mater.* **2018**, *8* (25), 1801090.
- (98) Li, W.; Wang, K.; Zhou, M.; Zhan, H.; Cheng, S.; Jiang, K. Advanced Low–Cost, High–Voltage, Long–Life Aqueous Hybrid Sodium/Zinc Batteries Enabled by a Dendrite–Free Zinc Anode and Concentrated Electrolyte. *ACS Appl. Mater. Interfaces* **2018**, *10* (26), 22059–22066.
- (99) Wang, R.; Jia, Y.; Kong, Z.; Wang, W.; Hu, Y.; Wang, G. Stabilization Strategies for Zinc Anode Interfaces under High Discharge Depth. *J. Energy Storage* **2025**, *105*, 114642.
- (100) Zhao, Z.; Wang, R.; Peng, C.; Chen, W.; Wu, T.; Hu, B.; Weng, W.; Yao, Y.; Zeng, J.; Chen, Z.; Liu, P.; Liu, Y.; Li, G.; Guo, J.; Lu, H.; Guo, Z. Horizontally Arranged Zinc Platelet Electrodeposits

- Modulated by Fluorinated Covalent Organic Framework Film for High-Rate and Durable Aqueous Zinc Ion Batteries. *Nat. Commun.* **2021**, *12* (1), 6606.
- (101) Zhao, J.; Ying, Y.; Wang, G.; Hu, K.; Yuan, Y. D.; Ye, H.; Liu, Z.; Lee, J. Y.; Zhao, D. Covalent Organic Framework Film Protected Zinc Anode for Highly Stable Rechargeable Aqueous Zinc-Ion Batteries. *Energy Storage Mater.* **2022**, *48*, 82–89.
- (102) Hao, J.; Li, X.; Zhang, S.; Yang, F.; Zeng, X.; Zhang, S.; Bo, G.; Wang, C.; Guo, Z. Designing Dendrite-Free Zinc Anodes for Advanced Aqueous Zinc Batteries. *Adv. Funct. Mater.* **2020**, *30* (30), 2001263.
- (103) Zeng, X.; Xie, K.; Liu, S.; Zhang, S.; Hao, J.; Liu, J.; Pang, W. K.; Liu, J.; Rao, P.; Wang, Q.; Mao, J.; Guo, Z. Bio-Inspired Design of an *in Situ* Multifunctional Polymeric Solid-Electrolyte Interphase for Zn Metal Anode Cycling at 30 mA Cm^{-2} and 30 mA h Cm^{-2} . *Energy Environ. Sci.* **2021**, *14* (11), 5947–5957.
- (104) Zhu, X.; Wang, K.; Xu, Y.; Zhang, G.; Li, S.; Li, C.; Zhang, X.; Sun, X.; Ge, X.; Ma, Y. Strategies to Boost Ionic Conductivity and Interface Compatibility of Inorganic – Organic Solid Composite Electrolytes. *Energy Storage Mater.* **2021**, *36*, 291–308.
- (105) Liu, X.; Ma, Q.; Shi, M.; Han, Q.; Liu, C. A Biomimetic Polymer–Clay Nanocomposite Coating for Dendrite-Free Zn Metal Anode. *Chem. Eng. J.* **2023**, *456*, 141016.
- (106) Cui, Y.; Zhao, Q.; Wu, X.; Chen, X.; Yang, J.; Wang, Y.; Qin, R.; Ding, S.; Song, Y.; Wu, J.; Yang, K.; Wang, Z.; Mei, Z.; Song, Z.; Wu, H.; Jiang, Z.; Qian, G.; Yang, L.; Pan, F. An Interface-Bridged Organic–Inorganic Layer That Suppresses Dendrite Formation and Side Reactions for Ultra-Long-Life Aqueous Zinc Metal Anodes. *Angew. Chem. Int. Ed.* **2020**, *59* (38), 16594–16601.
- (107) Gao, Y.; Yang, N.; Bu, F.; Cao, Q.; Pu, J.; Wang, Y.; Meng, T.; Chen, J.; Zhao, W.; Guan, C. Double-Sided Engineering for Space-Confining Reversible Zn Anodes. *Energy Environ. Sci.* **2024**, *17* (5), 1894–1903.
- (108) Zhang, M.; Li, J. –; Tang, Y.; Wang, D. –; Hu, H.; Liu, M.; Xiao, B.; Wang, P. –. Selective Zn–Ion Channels Enabled by a Double-Network Protective Layer for Stable Zinc Anode. *Energy Storage Mater.* **2024**, *65*, 103113.
- (109) Li, S.; Zhi, C. Versatile Biopolymers for Advanced Lithium and Zinc Metal Batteries. *Adv. Mater.* **2024**, 2413515.
- (110) Chang, C.; Hu, S.; Li, T.; Zeng, F.; Wang, D.; Guo, S.; Xu, M.; Liang, G.; Tang, Y.; Li, H.; Han, C.; Cheng, H.-M. A Robust Gradient Solid Electrolyte Interphase Enables Fast Zn Dissolution and Deposition Dynamics. *Energy Environ. Sci.* **2024**, *17* (2), 680–694.
- (111) Zhang, Y.; Wang, R.; Ao, H.; Ma, T.; Zhu, X.; Zhang, X.; Rong, J.; Zhou, Z.; Bai, Z.; Dou, S. X.; Wang, N.; Li, Z. Zn²⁺-Rich Chelate Layer Facilitates Ultrahigh-Rate Zinc Anodes Via Cation Compensation and Anion Repulsion. *Adv. Energy Mater.* **2025**, *15* (18), 2404203.
- (112) Boisset, A.; Menne, S.; Jacquemin, J.; Balducci, A.; Anouti, M. Deep Eutectic Solvents Based on N-Methylacetamide and a Lithium Salt as Suitable Electrolytes for Lithium–Ion Batteries. *Phys. Chem. Chem. Phys.* **2013**, *15* (46), 20054.
- (113) Qiu, H.; Du, X.; Zhao, J.; Wang, Y.; Ju, J.; Chen, Z.; Hu, Z.; Yan, D.; Zhou, X.; Cui, G. Zinc Anode-Compatible *in-Situ* Solid Electrolyte Interphase via Cation Solvation Modulation. *Nat. Commun.* **2019**, *10* (1), 5374.
- (114) Kasiri, G.; Trócoli, R.; Bani Hashemi, A.; La Mantia, F. An Electrochemical Investigation of the Aging of Copper Hexacyanoferrate during the Operation in Zinc–Ion Batteries. *Electrochim. Acta* **2016**, *222*, 74–83.
- (115) Wu, J.; Liang, Q.; Yu, X.; Lü, Q.; Ma, L.; Qin, X.; Chen, G.; Li, B. Deep Eutectic Solvents for Boosting Electrochemical Energy Storage and Conversion: A Review and Perspective. *Adv. Funct. Mater.* **2021**, *31* (22), 2011102.
- (116) Han, M.; Zhou, J.; Fan, H. J. Opportunity for Eutectic Mixtures in Metal–Ion Batteries. *Trends Chem.* **2023**, *5* (3), 214–224.
- (117) Zhang, C.; Zhang, L.; Yu, G. Eutectic Electrolytes as a Promising Platform for Next-Generation Electrochemical Energy Storage. *Acc. Chem. Res.* **2020**, *53* (8), 1648–1659.
- (118) Geng, L.; Wang, X.; Han, K.; Hu, P.; Zhou, L.; Zhao, Y.; Luo, W.; Mai, L. Eutectic Electrolytes in Advanced Metal–Ion Batteries. *ACS Energy Lett.* **2022**, *7* (1), 247–260.
- (119) Yang, W.; Du, X.; Zhao, J.; Chen, Z.; Li, J.; Xie, J.; Zhang, Y.; Cui, Z.; Kong, Q.; Zhao, Z.; Wang, C.; Zhang, Q.; Cui, G. Hydrated Eutectic Electrolytes with Ligand–Oriented Solvation Shells for Long–Cycling Zinc–Organic Batteries. *Joule* **2020**, *4* (7), 1557–1574.
- (120) Guan, K.; Chen, W.; Yang, Y.; Ye, F.; Hong, Y.; Zhang, J.; Gu, Q.; Wu, Y.; Hu, L. A Dual Salt/Dual Solvent Electrolyte Enables Ultrahigh Utilization of Zinc Metal Anode for Aqueous Batteries. *Adv. Mater.* **2024**, *36* (38), 2405889.
- (121) Khan, Z.; Kumar, D.; Crispin, X. Does Water-in-Salt Electrolyte Subdue Issues of Zn Batteries? *Adv. Mater.* **2023**, *35* (36), 2300369.
- (122) Suo, L.; Borodin, O.; Gao, T.; Olguin, M.; Ho, J.; Fan, X.; Luo, C.; Wang, C.; Xu, K. “Water-in-Salt” Electrolyte Enables High-Voltage Aqueous Lithium–Ion Chemistries. *Science* **2015**, *350* (6263), 938–943.
- (123) Wei, J.; Zhang, P.; Sun, J.; Liu, Y.; Li, F.; Xu, H.; Ye, R.; Tie, Z.; Sun, L.; Jin, Z. Advanced Electrolytes for High-Performance Aqueous Zinc–Ion Batteries. *Chem. Soc. Rev.* **2024**, *53* (20), 10335–10369.
- (124) Zhu, Y.; Yin, J.; Zheng, X.; Emwas, A.-H.; Lei, Y.; Mohammed, O. F.; Cui, Y.; Alshareef, H. N. Concentrated Dual-Cation Electrolyte Strategy for Aqueous Zinc–Ion Batteries. *Energy Environ. Sci.* **2021**, *14* (8), 4463–4473.
- (125) Yang, C.; Xia, J.; Cui, C.; Pollard, T.; Vatamanu, J.; Faraone, A.; Dura, J. A.; Tyagi, M.; Kattan, A.; Thimsen, E.; Xu, J. All-Temperature Zinc Batteries with High-Entropy Aqueous Electrolyte. *Nat. Sustain.* **2023**, *6* (3), 325–335.
- (126) Zhang, Q.; Ma, Y.; Lu, Y.; Zhou, X.; Lin, L.; Li, L.; Yan, Z.; Zhao, Q.; Zhang, K.; Chen, J. Designing Anion-Type Water-Free Zn²⁺ Solvation Structure for Robust Zn Metal Anode. *Angew. Chem. Int. Ed.* **2021**, *60* (43), 23357–23364.
- (127) Geng, X.; Hou, X.; He, X.; Fan, H. J. Challenges and Strategies on Interphasial Regulation for Aqueous Rechargeable Batteries. *Adv. Energy Mater.* **2024**, *14* (12), 2304094.
- (128) Dong, D.; Wang, T.; Sun, Y.; Fan, J.; Lu, Y.-C. Hydroscopic Solubilization of Zinc Acetates for Sustainable Aqueous Battery Electrolytes. *Nat. Sustain.* **2023**, *6* (11), 1474–1484.
- (129) Xie, J.; Liang, Z.; Lu, Y.-C. Molecular Crowding Electrolytes for High-Voltage Aqueous Batteries. *Nat. Mater.* **2020**, *19* (9), 1006–1011.
- (130) Dong, D.; Xie, J.; Liang, Z.; Lu, Y.-C. Tuning Intermolecular Interactions of Molecular Crowding Electrolyte for High-Performance Aqueous Batteries. *ACS Energy Lett.* **2022**, *7* (1), 123–130.
- (131) Wei, J.; Zhang, P.; Shen, T.; Liu, Y.; Dai, T.; Tie, Z.; Jin, Z. Supramolecule-Based Excluded-Volume Electrolytes and Conjugated Sulfonamide Cathodes for High-Voltage and Long–Cycling Aqueous Zinc–Ion Batteries. *ACS Energy Lett.* **2023**, *8* (1), 762–771.
- (132) Wang, X.; Wang, B.; Lei, P.; Wang, X.; Zhou, L.; Zhang, J.; Zhang, J.; Cheng, J. Polycation–Regulated Hydrogel Electrolytes with Nanoscale Hydrophobic Confinement Inducing Zn(002) Deposition for Highly Reversible Zinc Anodes. *Energy Environ. Sci.* **2024**, *17* (18), 6640–6655.
- (133) Hao, J.; Yuan, L.; Ye, C.; Chao, D.; Davey, K.; Guo, Z.; Qiao, S. Boosting Zinc Electrode Reversibility in Aqueous Electrolytes by Using Low-Cost Antisolvents. *Angew. Chem. Int. Ed.* **2021**, *60* (13), 7366–7375.
- (134) Wang, S.; Chen, S.; Ying, Y.; Li, G.; Wang, H.; Cheung, K. K.; Meng, Q.; Huang, H.; Ma, L.; Zapien, J. A. Fast Reaction Kinetics and Commendable Low-Temperature Adaptability of Zinc Batteries Enabled by Aprotic Water-Acetamide Symbiotic Solvation Sheath. *Angew. Chem. Int. Ed.* **2024**, *63* (8), No. e202316841.

- (135) Wang, S.; Liu, G.; Wan, W.; Li, X.; Li, J.; Wang, C. Acetamide-Caprolactam Deep Eutectic Solvent-Based Electrolyte for Stable Zn-Metal Batteries. *Adv. Mater.* **2024**, *36* (5), 2306546.
- (136) Chen, R.; Zhang, C.; Li, J.; Du, Z.; Guo, F.; Zhang, W.; Dai, Y.; Zong, W.; Gao, X.; Zhu, J.; Zhao, Y.; Wang, X.; He, G. A Hydrated Deep Eutectic Electrolyte with Finely-Tuned Solvation Chemistry for High-Performance Zinc–Ion Batteries. *Energy Environ. Sci.* **2023**, *16* (6), 2540–2549.
- (137) Zhong, Y.; Xie, X.; Zeng, Z.; Lu, B.; Chen, G.; Zhou, J. Triple-function Hydrated Eutectic Electrolyte for Enhanced Aqueous Zinc Batteries. *Angew. Chem. Int. Ed.* **2023**, *62* (40), No. e202310577.
- (138) Wan, J.; Wang, R.; Liu, Z.; Zhang, S.; Hao, J.; Mao, J.; Li, H.; Chao, D.; Zhang, L.; Zhang, C. Hydrated Eutectic Electrolyte Induced Bilayer Interphase for High-Performance Aqueous Zn-Ion Batteries with 100 °C Wide-Temperature Range. *Adv. Mater.* **2024**, *36* (11), 2310623.
- (139) Wang, F.; Borodin, O.; Gao, T.; Fan, X.; Sun, W.; Han, F.; Faraone, A.; Dura, J. A.; Xu, K.; Wang, C. Highly Reversible Zinc Metal Anode for Aqueous Batteries. *Nat. Mater.* **2018**, *17* (6), 543–549.
- (140) Clarisza, A.; Bezab, H. K.; Jiang, S.-K.; Huang, C.-J.; Olbasa, B. W.; Wu, S.-H.; Su, W.-N.; Hwang, B. J. Highly Concentrated Salt Electrolyte for a Highly Stable Aqueous Dual–Ion Zinc Battery. *ACS Appl. Mater. Interfaces* **2022**, *14* (32), 36644–36655.
- (141) Ji, Y.; Xie, J.; Shen, Z.; Liu, Y.; Wen, Z.; Luo, L.; Hong, G. Advanced Zinc–Iodine Batteries with Ultrahigh Capacity and Superior Rate Performance Based on Reduced Graphene Oxide and Water-in-Salt Electrolyte. *Adv. Funct. Mater.* **2023**, *33* (10), 2210043.
- (142) Li, S.; Zhang, Z.; Wu, J.; Guo, X.; Chen, Y.; Wang, C.; Yu, F.; Wang, Z.; Li, D.; Chen, Y. Stable Zn–WO₃ Battery with a ZnCl₂ Water-in-Salt Electrolyte. *J. Power Sources* **2023**, *560*, 232691.
- (143) Li, C.; Kingsbury, R.; Thind, A. S.; Shyamsunder, A.; Fister, T. T.; Klie, R. F.; Persson, K. A.; Nazar, L. F. Enabling Selective Zinc–Ion Intercalation by a Eutectic Electrolyte for Practical Anodeless Zinc Batteries. *Nat. Commun.* **2023**, *14* (1), 3067.
- (144) Ren, H.; Li, S.; Wang, B.; Zhang, Y.; Wang, T.; Lv, Q.; Zhang, X.; Wang, L.; Han, X.; Jin, F.; Bao, C.; Yan, P.; Zhang, N.; Wang, D.; Cheng, T.; Liu, H.; Dou, S. Molecular-Crowding Effect Mimicking Cold-Resistant Plants to Stabilize the Zinc Anode with Wider Service Temperature Range. *Adv. Mater.* **2023**, *35* (1), 2208237.
- (145) Cao, Z.; Zhu, X.; Gao, S.; Xu, D.; Wang, Z.; Ye, Z.; Wang, L.; Chen, B.; Li, L.; Ye, M.; Shen, J. Ultrastable Zinc Anode by Simultaneously Manipulating Solvation Sheath and Inducing Oriented Deposition with PEG Stability Promoter. *Small* **2022**, *18* (6), 2103345.
- (146) Ciurdac, D. E.; Cruz, C. D. L.; Patil, N.; Mavrandonakis, A.; Marcilla, R. Molecular Crowding Bi–Salt Electrolyte for Aqueous Zinc Hybrid Batteries. *Energy Storage Mater.* **2022**, *53*, 532–543.
- (147) Wei, L.; Chen, Y.; Huang, Z.; Zheng, S.; Guo, X. Redox-Enhanced Zinc–Ion Hybrid Capacitors with High Energy Density Enabled by High–Voltage Active Aqueous Electrolytes Based on Low Salt Concentration. *Energy Storage Mater.* **2023**, *58*, 30–39.
- (148) Lin, Y.; Wang, S.; Huang, J.; Chen, L.; Bi, T.; Qi, L.; Cai, Z.; Zeng, X.; Hu, P.; Chen, W.; Yu, L.; Chen, C. Coupling of Mechanical, Self-Healing, Adhesion, and High-Ion Conducting Properties in Anti-Freezing Hydrogel Electrolytes of Zinc Ion Batteries via Fe³⁺-Carboxylate Coordination. *Adv. Funct. Mater.* **2025**, 2504726.
- (149) Liu, Y.; Li, F.; Hao, J.; Li, H.; Zhang, S.; Mao, J.; Zhou, T.; Wang, R.; Zhang, L.; Zhang, C. A Polyanionic Hydrogel Electrolyte with Ion Selective Permeability for Building Ultra-Stable Zn/I₂ Batteries with 100 °C Wide Temperature Range. *Adv. Funct. Mater.* **2024**, *34* (29), 2400517.
- (150) Qin, S.; Qi, R.; Wang, Y.; Hu, Y.; Ma, M.; Luan, Y.; Yang, H.; Yang, K. A Jointly Triggered H₂ Evolution Model Modulated Polyanionic Hydrogel Electrolyte for Reversible Zn Chemistry. *Adv. Funct. Mater.* **2025**, 2505946.
- (151) Wang, X.; Lei, P.; Zheng, C.; Wang, Z.; Wang, B.; Cui, X.; Cheng, J. Flexible and Durable Meter-Long Fiber-Shaped Zn-Ion Battery Enabled by Zincophilic, Tough Double-Network Hydrogel Electrolytes. *Adv. Funct. Mater.* **2025**, 2500916.
- (152) Zhang, H.; Gan, X.; Yan, Y.; Zhou, J. A Sustainable Dual Cross-Linked Cellulose Hydrogel Electrolyte for High–Performance Zinc–Metal Batteries. *Nano–Micro Lett.* **2024**, *16* (1), 106.
- (153) He, Q.; Zhong, Y.; Li, J.; Chai, S.; Yang, Y.; Liang, S.; Chang, Z.; Fang, G.; Pan, A. Constructing Kosmotropic Salt-Compatible PVA Hydrogels for Stable Zinc Anodes via Strong Hydrogen Bonds Preshielding Effect. *Adv. Energy Mater.* **2024**, *14* (23), 2400170.
- (154) Kim, M.; Shin, S.; Lee, J.; Park, Y.; Kim, Y.; Kim, H.; Choi, J. W. Cationic Additive with a Rigid Solvation Shell for High-Performance Zinc Ion Batteries. *Angew. Chem. Int. Ed.* **2022**, *61* (47), No. e202211589.
- (155) Wang, P.; Xie, X.; Xing, Z.; Chen, X.; Fang, G.; Lu, B.; Zhou, J.; Liang, S.; Fan, H. J. Mechanistic Insights of Mg²⁺-Electrolyte Additive for High-Energy and Long-Life Zinc-Ion Hybrid Capacitors. *Adv. Energy Mater.* **2021**, *11* (30), 2101158.
- (156) Zhao, R.; Wang, H.; Du, H.; Yang, Y.; Gao, Z.; Qie, L.; Huang, Y. Lanthanum Nitrate as Aqueous Electrolyte Additive for Favourable Zinc Metal Electrodeposition. *Nat. Commun.* **2022**, *13* (1), 3252.
- (157) Zhu, M.; Wang, X.; Tang, H.; Wang, J.; Hao, Q.; Liu, L.; Li, Y.; Zhang, K.; Schmidt, O. G. Antifreezing Hydrogel with High Zinc Reversibility for Flexible and Durable Aqueous Batteries by Cooperative Hydrated Cations. *Adv. Funct. Mater.* **2020**, *30* (6), 1907218.
- (158) Wan, F.; Zhang, L.; Dai, X.; Wang, X.; Niu, Z.; Chen, J. Aqueous Rechargeable Zinc/Sodium Vanadate Batteries with Enhanced Performance from Simultaneous Insertion of Dual Carriers. *Nat. Commun.* **2018**, *9* (1), 1656.
- (159) Li, Q.; Ma, K.; Hong, C.; Yang, Z.; Qi, C.; Yang, G.; Wang, C. High–Voltage K/Zn Dual–Ion Battery with 100,000–Cycles Life Using Zero–Strain ZnHCF Cathode. *Energy Storage Mater.* **2021**, *42*, 715–722.
- (160) Zhu, Z.; Tsai, H.; Parker, S. T.; Lee, J. –; Yabuuchi, Y.; Jiang, H. Z. H.; Wang, Y.; Xiong, S.; Forse, A. C.; Dinakar, B.; Huang, A.; Dun, C.; Milner, P. J.; Smith, A.; Guimaraes Martins, P.; Meihaus, K. R.; Urban, J. J.; Reimer, J. A.; Neaton, J. B.; Long, J. R. High-Capacity, Cooperative CO₂ Capture in a Diamine–Appended Metal–Organic Framework through a Combined Chemisorptive and Physisorptive Mechanism. *J. Am. Chem. Soc.* **2024**, *146* (9), 6072–6083.
- (161) Luo, Z.; Xia, Y.; Chen, S.; Wu, X.; Zeng, R.; Zhang, X.; Pan, H.; Yan, M.; Shi, T.; Tao, K.; et al. Synergistic “Anchor–Capture” Enabled by Amino and Carboxyl for Constructing Robust Interface of Zn Anode. *Nano–Micro Lett.* **2023**, *15* (1), 205.
- (162) Tan, H.; Meng, C.; Sun, T.; Wu, X.-L.; Liu, H.; Wang, J.-J. Boosting Zinc Anode Durability through Synergistic Inner Helmholtz Plane and Interfacial Electric Field Regulation. *Sci. Bull.* **2024**, *69* (13), 2025–2029.
- (163) Wei, X.; Mu, Y.; Chen, J.; Zhou, Y.; Chu, Y.; Yang, L.; Huang, C.; Xue, T.; Zang, L.; Yang, C.; Zeng, L. Optimizing Zn (100) Deposition via Crystal Plane Shielding Effect towards Ultra-High Rate and Stable Zinc Anode. *Energy Storage Mater.* **2025**, *75*, 104026.
- (164) Li, H.; Ren, Y.; Zhu, Y.; Tian, J.; Sun, X.; Sheng, C.; He, P.; Guo, S.; Zhou, H. A Bio-Inspired Trehalose Additive for Reversible Zinc Anodes with Improved Stability and Kinetics. *Angew. Chem. Int. Ed.* **2023**, *62* (41), No. e202310143.
- (165) Shang, Y.; Kundu, V.; Pal, I.; Kim, H. N.; Zhong, H.; Kumar, P.; Kundu, D. Highly Potent and Low-Volume Concentration Additives for Durable Aqueous Zinc Batteries: Machine Learning-Enabled Performance Rationalization. *Adv. Mater.* **2024**, *36* (9), 2309212.
- (166) Lin, Y.; Mai, Z.; Liang, H.; Li, Y.; Yang, G.; Wang, C. Dendrite-Free Zn Anode Enabled by Anionic Surfactant–Induced Horizontal Growth for Highly-Stable Aqueous Zn–Ion Pouch Cells. *Energy Environ. Sci.* **2023**, *16* (2), 687–697.
- (167) Yan, T.; Tao, M.; Liang, J.; Zheng, G.; Wu, B.; Du, L.; Cui, Z.; Song, H. Refining the Inner Helmholtz Plane Adsorption for

Achieving a Stable Solid–Electrolyte Interphase in Reversible Aqueous Zn–Ion Pouch Cells. *Energy Storage Mater.* **2024**, *65*, 103190.

(168) Li, Y.; Zheng, X.; Carlson, E. Z.; Xiao, X.; Chi, X.; Cui, Y.; Greenburg, L. C.; Zhang, G.; Zhang, E.; Liu, C.; Yang, Y.; Kim, M. S.; Feng, G.; Zhang, P.; Su, H.; Guan, X.; Zhou, J.; Wu, Y.; Xue, Z.; Li, W.; Bajdich, M.; Cui, Y. In Situ Formation of Liquid Crystal Interphase in Electrolytes with Soft Templating Effects for Aqueous Dual–Electrode–Free Batteries. *Nat. Energy* **2024**, *9* (11), 1350–1359.

(169) Zhao, X.; Wang, Y.; Huang, C.; Gao, Y.; Huang, M.; Ding, Y.; Wang, X.; Si, Z.; Zhou, D.; Kang, F. Tetraphenylporphyrin-based Chelating Ligand Additive as a Molecular Sieving Interfacial Barrier toward Durable Aqueous Zinc Metal Batteries. *Angew. Chem. Int. Ed.* **2023**, *62* (46), No. e202312193.

(170) Liu, H.; Xin, Z.; Cao, B.; Xu, Z.; Xu, B.; Zhu, Q.; Yang, J.; Zhang, B.; Fan, H. J. Polyhydroxylated Organic Molecular Additives for Durable Aqueous Zinc Battery. *Adv. Funct. Mater.* **2024**, *34* (4), 2309840.

(171) Gao, Y.; Yuan, Y.; Huang, S.; Yao, N.; Yu, L.; Chen, Y.; Zhang, Q.; Chen, X. A Knowledge–Data Dual-Driven Framework for Predicting the Molecular Properties of Rechargeable Battery Electrolytes. *Angew. Chem. Int. Ed.* **2025**, *64* (4), No. e202416506.

(172) Meng, Q.; Huang, Y.; Li, L.; Wu, F.; Chen, R. Smart Batteries for Powering the Future. *Joule* **2024**, *8* (2), 344–373.

(173) Zheng, W.; Liang, G.; Liu, Q.; Li, J.; Yuwono, J. A.; Zhang, S.; Peterson, V. K.; Guo, Z. The Promise of High–Entropy Materials for High–Performance Rechargeable Li–Ion and Na–Ion Batteries. *Joule* **2023**, *7* (12), 2732–2748.

(174) Zhang, F.; Liao, T.; Qi, D.-C.; Wang, T.; Xu, Y.; Luo, W.; Yan, C.; Jiang, L.; Sun, Z. Zn–Ion Ultrafluidity via Bioinspired Ion Channel for Ultralong Lifespan Zn–Ion Battery. *Natl. Sci. Rev.* **2024**, *11* (8), nwae199.

(175) Lombardo, T.; Duquesnoy, M.; El–bouysidy, H.; Åréen, F.; Gallo–bueno, A.; Jørgensen, P. B.; Bhowmik, A.; Demortière, A.; Ayerbe, E.; Alcaide, F.; et al. Artificial Intelligence Applied to Battery Research: Hype or Reality? *Chem. Rev.* **2022**, *122* (12), 10899–10969.